FFI-RAPPORT

16/01321

MODITIC

report on source term modelling

–
Stephane Burkhart (Direction Générale de l'Armement - DGA)
Oscar Björnham (Totalförsvarets forskningsinstitut - FOI)
Thomas Vik (Forsvarets forskningsinstitutt - FFI)
Guillaume Leroy (Institut National de l'Environnement Industriel et des RISques - INERIS)

MODITIC

report on source term modelling

Stephane Burkhart (Direction Générale de l'Armement - DGA)
Oscar Björnham (Totalförsvarets forskningsinstitut - FOI)
Thomas Vik (Forsvarets forskningsinstitutt - FFI)
Guillaume Leroy (Institut National de l'Environnement Industriel et des RISques - INERIS)

Norwegian Defence Research Establishment (FFI) 13 October 2016

Keywords

EDA
Amoniakk
Modellering og simulering
Spredning

FFI-rapport
FFI-RAPPORT 16/01321

Project number
1392

ISBN
P: 978-82-464-2828-4
E: 978-82-464-2829-1

Approved by
Hanne Breivik, *Research Manager*
Janet Martha Blatny, *Director*

Summary

The European Defence Agency (EDA) project B-1097-ESM4-GP “MOdelling the DIspersion of Toxic Industrial Chemicals in urban environments” (MODITIC) has in the period from 2012 to 2016 studied the release and transport of neutral and non-neutral chemicals in complex urban environments, in order to enhance the understanding of the dominating physical processes involved, and to support improvements in modelling techniques. WP3000 concerns agent characterization and source modelling, this includes modelling the flashing, expansion, evaporation and rainout processes.

Four studies have been conducted within WP3000 by four research institutes:

- DGA tested Reynolds-averaged Navier-Stokes models for simulating the release of a pure gas or two-phase ammonia jet impinging an obstacle. The small time step required makes this method inappropriate for large geometrical domains. In addition, unphysical results for some parameters were obtained.
- FFI used large eddy simulations approaches for the same two cases. The demands for the time step size and the grid resolution is even stricter in this case, precluding simulation of the entire experimental duration, as well as for large domains. Furthermore, in order to calculate the flashing of the liquid jet and the evaporation of the liquid droplets, a two-way coupling between the gas phase solver and the Lagrangian liquid droplet solver is needed, but the model used does not include such a two-way coupling at the present time.
- FOI tested an approach where the conditions in the jet are calculated by an analytical approach and given as input to a subsequent computational fluid dynamics (CFD) simulation of the dispersion of gas and droplets. They validated the approach with field tests of the release and dispersion of liquified ammonia, and the results are encouraging.
- Finally, INERIS used a large eddy simulations approach where the inlet conditions is specified from real (experimental) energy spectrum profiles. The vapour source term is specified according to an analytical calculation. The simulations are compared with field experiments of the release of ammonia, and the results are promising regarding the complexity for describing both near and far field dispersion.

None of the institutes involved in MODITIC have a CFD capability that can fully model all the physical processes associated with a two-phase release of ammonia. The CFD methodologies produced somewhat unphysical results. In addition, the computer resources needed for a full CFD simulation makes such models inappropriate for large domains. On the other hand, a decoupled approach, where the rapid processes (flashing and expansion of the jet) are calculated with an empirical or analytical approach, and the slow processes (gas dispersion and air entrainment) are simulated with CFD, yields encouraging results. It is recommended to use the decoupled approach when modelling such demanding processes.

Sammendrag

European Defence Agency-prosjektet B-1097-ESM4-GP MODITIC (MOdelling the Dispersion of Toxic Industrial Chemicals in urban environments) har i perioden 2012 – 2016 studert utslipp og spredning av nøytrale og ikke-nøytrale industrikjemikalier i urbane miljø. Målene er både å øke kunnskapen om de dominerende fysikalske prosessene som er involvert, og å støtte opp om forbedring av modelleringsteknikker. Arbeidspakke WP3000 dreier seg om beskrivelse av utslippskilden. Dette inkluderer beskrivelse av såkalt "flashing", utvidelse av væsken og gassen etter utslippet, fordamping og væskedamdannelse.

Fire studier er gjenomført innenfor WP3000 av fire forskningsinstitutt:

- DGA brukte Reynolds-averaged Navier-Stokes-modeller for å studere utslipp av ammoniakk som gass og som tofase der utslippsstrømmen treffer en vegg. Tidsstegene som var nødvendige for simuleringene, var imidlertid så små at metoden er uegnet for store geometriske domener. I tillegg resulterte metoden i ufysikalske verdier på en del variabler.
- FFI brukte large eddy-simuleringer for de samme to scenarioene. Disse metodene har imidlertid enda sterkere krav til tidssteget og størrelsen på beregningsgrid, slik at det ble uhåndterlig å simulere hele eksperimentet. Metodene blir også for tidkrevende for store geometriske domener. Modellen som ble testet, gir heller ikke mulighet til å simulere fullt ut de fysikalske prosessene som er involvert i flashing av væskestrømmen og fordamping av væskedråpene.
- FOI testet en metodikk der forholdene til jetstrømmen blir beregnet analytisk og gitt som inngangsparametre til en computational fluid dynamics-beregning (CFD) av den videre spredningen av gass. Simuleringene er sammenlignet med feltforsøk av utslipp og spredning av ammoniakk, og resultatene er lovende.
- INERIS har brukt en large eddy-simuleringsmetode der ingangsparametrene er spesifisert fra reelle (eksperimentelle) målinger av energispektrumsprofiler. Gasskilden er spesifisert fra en analytisk beregning. Simuleringene er sammenlignet med feltforsøk med utslipp av ammoniakk, og resultatene er lovende med tanke på å beskrive spredning både i nærfeltet og langt fra kilden.

Ingen av instituttene har en CFD-kapabilitet som fullt ut kan beskrive alle fysikalske prosesser med et tofaseutslipp av ammoniakk. CFD-modellene som er brukt, ga til dels ufysikalske resultater, i tillegg til at de er for tidkrevende å brukes på store geometriske domener. I stedet anbefales det å benytte en totrinnsmodell, der de raske prosessene (flashing og utvidelse at strømmen) beregnes analytisk, og de langsomme prosessene (transport av gass og innblanding av luft) simuleres med CFD. En slik framgangsmåte har vist lovende resultater.

Contents

Preface

This work is part of the European Defence Agency (EDA) project B-1097-ESM4-GP “MOdelling the DIspersion of Toxic Industrial Chemicals in urban environments” (MODITIC). The scientific objective of this project was the systematic study of the release and transport of neutral and non-neutral chemicals in complex urban environments, to enhance understanding of the dominating physical processes involved, and to support improvements in modelling techniques. The participating organisations were:

- Direction Générale de l’Armement (DGA), DGA CBRN Defence, France
- Institut National de l’Environnement Industriel et des Risques (INERIS), France
- Norwegian Defence Research Establishment (FFI), Norway
- Swedish Defence Research Agency (FOI), Sweden
- University of Surrey (UoS), United Kingdom

FFI was the lead organisation. The project was initiated 1 September 2012 and terminated 1 March 2016. The project was funded by the Norwegian Ministry of Defence, the Swedish Ministry of Defence, the French Ministry of Defence, and the French Ministry of Ecology, Sustainability and Energy.

This report describes work and results for WP3000 “Source Term Modelling”. Chapter 2 is authored by Direction Générale de l’Armement (DGA), chapter 3 the by FFI, chapter 4 by the Swedish Defence Research Agency (FOI), and chapter 5 by Institut National de l’Environnement Industriel et des Risques (INERIS). Each institute has conducted a validation of the quality of their contribution. Stephane Burkhart (DGA) is the main author and combined the various contributions into a single report, while Thomas Vik (FFI) has transferred it to the FFI report template.

1 Introduction

1.1 Objectives

Toxic industrial gases are often stored under pressure in a liquid state in large tanks or vessels. A release from a pressurized tank can give rise to a dense gas that will disperse quite differently from a neutral gas.

Part of the released liquid forms a jet that undergoes a flashing process and part of it is spilled on the ground (rainout). Rainout to the ground may also appear when the jet impinges a wall. The liquid pools from rainout constitute secondary vapor sources. The jet is thus a complicated mixture of liquid aerosol, vapor and entrained air. There are many models that describe such a jet, which are formulated in several different ways [1, 2, 3, 4, 5, 6].

Gaussian and integral models for calculating the dispersion of gases were developed 40 years ago[7] and are still used for hazard predictions. Computational Fluid Dynamics (CFD) models, however, are capable of resolving the air and gas flow to a much finer level, and can therefore more accurately describe the dispersion for instance around obstructions.

The objective of the MODITIC project is to enhance the understanding of the dispersion of neutral and non-neutral[1] toxic industrial chemicals (TICs) in an urban area. WP3000 concerns agent characterization and source modelling and aims to use the current CFD model capabilities of the participating institutes to handle dense multiphase jets resulting from leakage from pressurized tanks impinging on obstacles. This includes modelling the flashing, expansion, evaporation and rainout processes. The ability of operational models to handle dense gas release is assessed in MODITIC WP6000 [8].

1.2 Experimental validation

For validation purposes, we refer to experimental data provided by INERIS and described in the MODITIC WE3300 report [9]:

- “Indoor case 2” with a release of ammonia gas.
- “Indoor case 4” with a two-phase ammonia release.
- “Outdoor case 4” with a two-phase release of ammonia.

In addition, results from the FLADIS experiments with the release of liquefied ammonia [10, 11] have been used for validation. The experimental setups are described in the chapters where they are used.

[1] A neutral gas has density equal to that of air while a non-neutral gas has a density different from that of air.

1.2.1 Output data available

Measurement of flow properties in the jet is indeed experimentally challenging. The experimental data available for comparison are limited to temperature and concentrations at selected spatial points. To perform the comparison, we have at disposal the following results:

- Gas concentration at the chosen experimental points
- Rainout (for the INERIS indoor cases)
- Gas temperature (for the INERIS indoor cases and the FLADIS field experiments)
- Concrete wall temperature (for the INERIS indoor cases)
- Ground temperature (for the INERIS outdoor case)

2 DGA CBRN Defence – RANS modelling of indoor ammonia releases

The release of ammonia as pure vapour and as a two-phase jet are simulated with a RANS approach, and compared with the results from the indoor INERIS experiments.

2.1 Geometrical description

The experimental setup is shown in figure 2.1. Some experimental data of interest as input for the chosen CFD simulations are summarized in table 2.1.

The test chamber is about 5 m × 4 m × 4 m = 80 m^3. The air inlet is at floor level with a diverting plate in order to prevent the flow from perturbing the jet, see figure 2.2. The air extraction is at the ceiling at the opposite wall from the inlet.

2.2 Simulation Strategy

Basically, the behaviour of ammonia gas (case 2) or liquid (case 4) released under pressure through a small aperture (nozzle 4 mm diameter) were modelled.

An intermediate description of the flow expanding from the pipe end is fairly straightforward for the gas and air mixture case, while slightly more complicated for the multiphase case (liquid droplets, gas and air mixture). We needed simple expressions for the flow velocity, pressure and temperature at the inlet (nozzle). In addition, for the multiphase case, we considered a droplet distribution, a gas mass fraction, and a distance where to apply these boundary conditions.

According to Duplantier [12] and the TNO yellow book [13], we can relate the quantities at the pipe end from those in the tank bottle: the liquid and gas follow an adiabatic process untill the end

Case 2 (gas)	**Tank**	**Nozzle**	**Ambient**
Temperature	T_T = 6.1 $^\circ C$	T_N = -6 $^\circ C$	HR = 88%, T_A = 5.6 $^\circ C$
Pressure	P_{sat} = 5.4 bar	P_N = 1.8 bar	
Flow rate/duration		$Q_m = 3.0 \cdot 10^{-3}$ kg/s duration = 533 s	2028m^3/h (extraction)
Case 4 (liquid + gas)	**Tank**	**Nozzle**	**Ambient**
Temperature	T_T = 8.1 $^\circ C$	T_N = -16 $^\circ C$	HR = 47%, T_A = 4.8 $^\circ C$
Pressure	P_{sat} = 5.1 bar	P_N = 2.0 bar	
Flow rate/duration		$Q_m = 1.44 \cdot 10^{-2}$ kg/s duration = 507s	1960 m^3/h (extraction)

Table 2.1 *Experimental inlet conditions for the chosen scenarios*

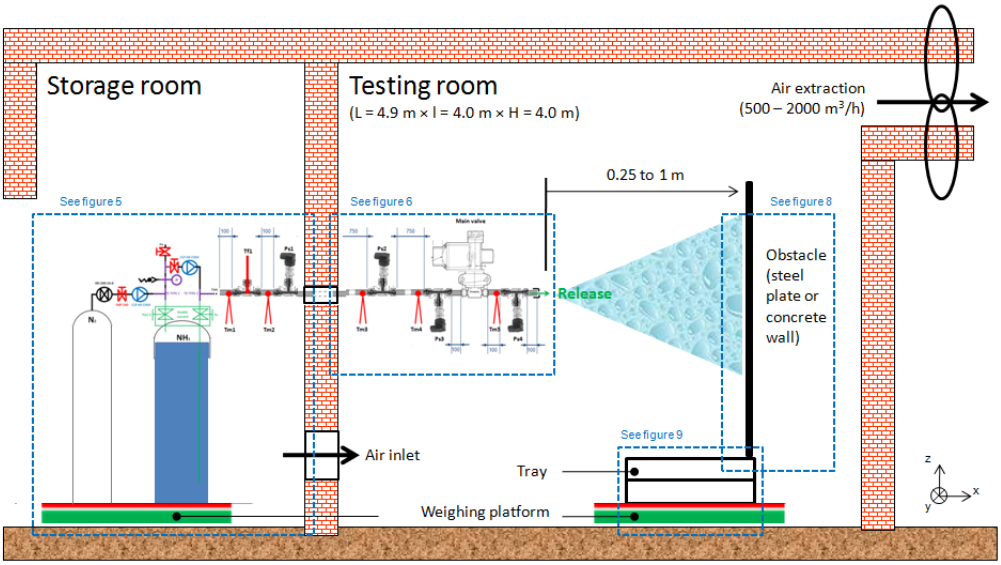

Figure 2.1 *Sketch of experimental device in the 80 m^3 trial chamber at INERIS. The pipe for the ammonia release extends 2 meters inside the testing room and has a diameter of 4 mm.*

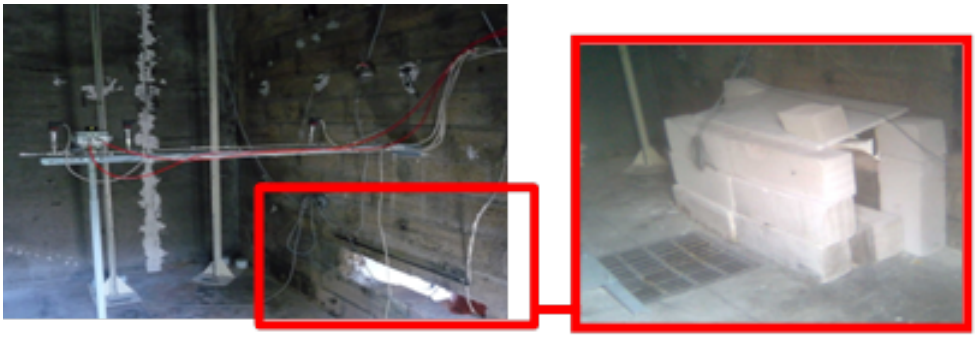

Figure 2.2 *The experimental air inlet and the diverting plate.*

of the pipe. Then a thermodynamic flash occurs in two steps: expansion and acceleration of the gas jet through an isenthalpic process (HEM method), and entrainment of surrounding air into the jet. We will then use a compressible Eulerian gas description in both cases, with a Lagrangian droplet phase superimposed for case 4.

2.2.1 Inlet conditions

Inlet conditions for case 2

From chapter 2 in [13], the velocity at the nozzle, U_e, can be estimated as:

$$U_e = Q_m/(\rho_v S) \tag{2.1}$$

where $Q_m = 3.1 \cdot 10^{-3}$ kg/s is the gas mass rate, $S = 1.26 \cdot 10^{-5}$ m^2 the nozzle surface area and ρ_v (-6 $^\circ C$) = 1.38 kg/m^3 is the density (perfect gas expression). This gives U_e = 172 m/s, which we took as inlet velocity in our simulation model. The sound velocity at this temperature is $c \sim \sqrt{\gamma RT/Mw}$ = 412 m/s, where $\gamma \sim$1.3 is the ratio of specific heats at constant pressure and constant volume, R the gas constant, and Mw the molecular weight.

From an isenthalpic expansion, we expect a velocity at the end of the expansion region (a few nozzle diameters long) of:

$$U_f = U_e + \Delta pS/Q_m \tag{2.2}$$

where $\Delta p = (1.8 - 1) = 0.8$ bar. We arrive at a value U_f = 508 m/s. This is well above the speed of sound!

We notice that in the Fluent software we used for the simulation, the compressible gas (solved nevertheless with pressure based solver) will be accelerated owing to the over-pressure as soon as the gas becomes supersonic. However, Fluent uses an adiabatic expression, instead of the isenthalpic expansion described here, resulting in a computed velocity at the end of the expansion region higher than 508 m/s.

The gas temperature is not expected to vary much from this isenthalpic expansion. This is also seen in the experiment where the gas temperature measured on the obstacle was 5 $^\circ C$ (slightly cooler than the ambient temperature).

For compressible gas flows, we need to put in the total temperature (the temperature at the given thermodynamic state if the fluid were brought to zero velocity) as a boundary condition, not the static temperature only (which is the temperature of the fluid). For incompressile flow, the static temperature equals the total temperature unless kinetic energy is explicitly added [14].

Inlet conditions for case 4

From the same references [13] we can infer the velocity at nozzle, quality (gas mass fraction), and droplet phase characteristics.

We took the same expression as above for the liquid phase before flashing (it is implicitly assumed that the flashing does not occur upstream in the pipe, but just at the exit).

$$U_e = Q_m/(\rho_l S) \tag{2.3}$$

ρ_l, liquid density (kg/m3)	653.1
C_{pl}, liquid heat capacity at constant pressure (J/kg/K)	4502.8
L_v, latent heat of vaporization (kJ/kg)	1306.31
T_b, boiling point (K)	-33.45
κ, thermal conductivity (W/m/K)	0.565
η, dynamic viscosity (Pa s)	$1.85 \cdot 10^{-4}$
γ, surface tension (N/m)	0.029
Mw, molecular weight (kg/kmol)	17.03

Table 2.2 *Physical properties of ammonia used in the modeling*

with $Q_m = 1.44 \cdot 10^{-2}$ kg/s and ρ_l(-16 °C) = 659.6 kg/m^3 we got $U_e = 1.73$ m/s.

The liquid flashes and gets accelerated as it changes density from liquid to gas:

$$U_f = U_e + \Delta pS/Q_m \tag{2.4}$$

With $\Delta p = (2 - 1) = 1$ bar, we got: $U_f = 89.23$ m/s.

We notice that sound velocity in the liquid phase is much higher ($c \sim 1361$ m/s at 5 °C for example).

From[12], we got the mean Sauter diameter, d_{32}, expressed from a critical We number which again depends on the nozzle diameter, d_p:

$$d_{32} = 133\lambda We^{-0.74} \tag{2.5}$$

where $We = \rho_l U_f^2 \lambda/\sigma = 87131$ is the Weber number, $\sigma = 0.03$ N/m the surface tension, $\lambda = d_p/8$ is the radial integral length scale at the jet exit based on fully developed turbulent pipe flow, and $d_p = 4 \cdot 10^{-3}$ m. We got: $d_{32} = 15$ mm.

We assume the droplet distribution will be lognormal. In Fluent, this is translated as a Rosin-Rammler cumulative distribution $P(d < d') = 1 - e^{-(d'/\overline{d})^n}$, where $\overline{d}$ is the size constant. We fitted this law with a cumulative log normal law, and found $\overline{d} = 2.7$ mm and $n = 2.7$.

Next, we needed the vapour pressure to calculate the evaporate of the droplets. For this, we filled the data base of Fluent for ammonia with the expression

$$P_{sat}(T) = A1 + A2T + A3T^2 + A4T^3 + \cdots \tag{2.6}$$

From another expression for the vapour pressure: $P_{sat}(T) = e^{(A+B/T+C\ln T+DT^E)}$ with $A = 90.483$, $B = -4669.7$, $C = -11.607$, $D = 0.017194$, $E = 1$ we got the coefficients:
$A1 = -2 \cdot 10^7$, $A2 = 304089$, $A3 = -1311.5$, $A4 = 1.9073$.

The other physical parameters taken for ammonia at a referece temperature of $T = 12$ °C are given in table 2.2.

Finally, we needed the quality (gas mass fraction) at the inlet, x_v. From [12] we got the expression:

$$x_v = C_{pl}\Delta T/L_v \tag{2.7}$$

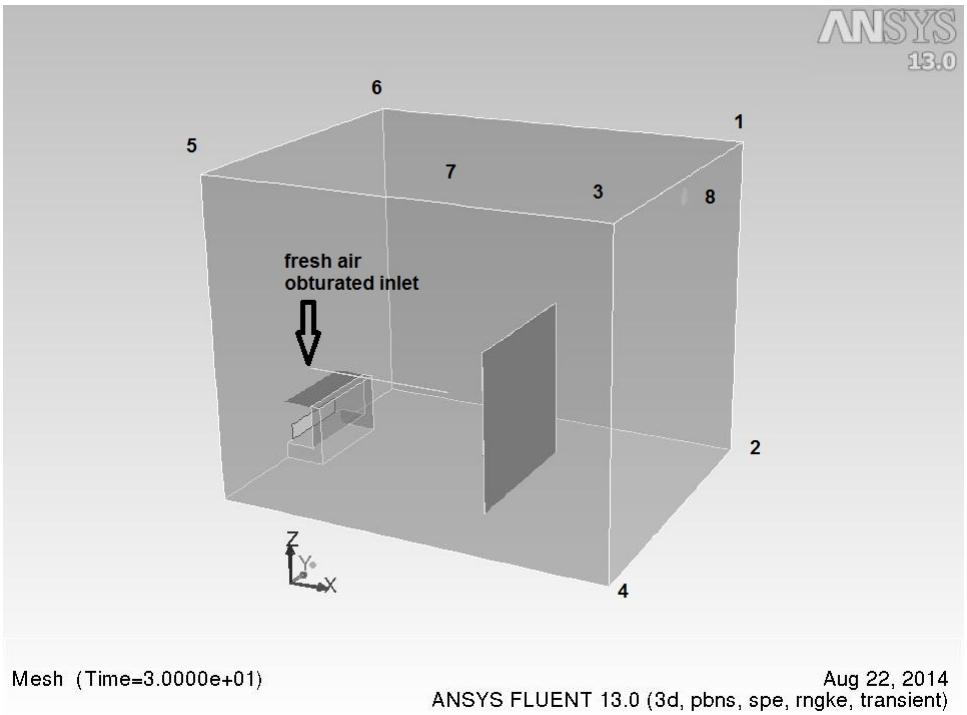

Figure 2.3 *CAD generated with Gambit Software for the simplified geometry.*

where ΔT is the temperature drop between tank and nozzle, that is $\Delta T = T_T - T_N = 24\ ^\circ C$. With the parameters in table 2.2. we got the vapor quality $x_v = 8.3$ %

We could now deduce the mass flow rates for the liquid (Q_{ml}) and vapour (Q_{mv}) phases respectively:

$$Q_{ml} = 91.7\%\ Q_m = 0.0132 \text{ kg/s}$$

$$Q_{mv} = 8.3\%\ Qm = 11.95 \cdot 10^{-4} \text{ kg/s}.$$

2.2.2 Meshing Procedure

The geometry was prepared with Gambit v2.4.6 software. We added the obstruction of the fresh air, the obstacle as a thin plate 3 meter from the wall and 1 meter from the nozzle (pipe exit). The sensors used to compare with experimental data are indicated on figure 2.3.

The mesh was also created with Gambit v2.4.6 and consisted of about 1.5 million tetrahedral cells of mixed type. The EquiAngleSkew quality factor is >0.9 (bad) in less than 0.02% of the cells, far from the nozzle (the bad cells are located close to fresh air inlet and in corners). We used size function to pre-mesh the small details. The smallest mesh sizes are about 0.8 mm (close to the pipe exit). Figure 2.4 shows the surface mesh on the wall supporting the pipe and fresh air inlet. The mesh was exported to Ansys-Fluent v13.0.

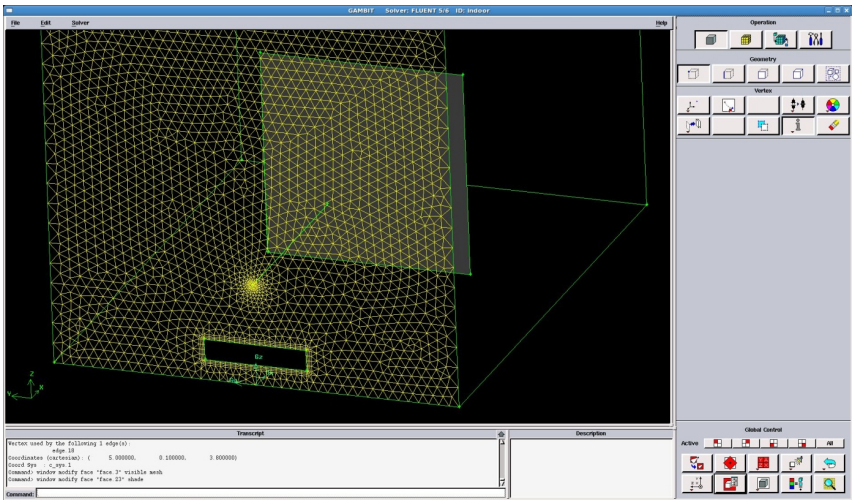

Figure 2.4 *Details of mesh on the wall supporting the pipe and fresh air inlet.*

2.2.3 Calculation setup and control

We used the unsteady k-ε renormalization-group (RNG) model for the turbulent flow, with second order discretisation for all but the scalar variables. The time step, dt, is based on highest velocity and smallest mesh size, that is about dt = 1 mm / 500 m/s = 2 μs. It took about 2500 iterations for the jet to stabilize, and further 30 s to reach a quasi-stationary state for the flow field (mean and turbulent parts). Then we froze the flow, and calculated the dispersion of the gas and droplets with a much larger time step (order of ms). The gas transport takes into account turbulent diffusion, and particle transport is driven by advection and a random walk algorithm based on local turbulence. Transfer of mass and heat is accounted for between droplets and gas mixture. It takes about 150 s to reach 63% of the final state (characteristic time).

2.3 Results

2.3.1 Results on case 2 (pure gas)

Figure 2.5 shows the concentration expressed in terms of percentage of the Lower Flammable Limit (LFL) of ammonia. LFL corresponds to a molar concentration of 150000 ppm = 0.15.

A striking difference between the simulation and the observed data is the much larger spread of experimental data.The observed concentrations are also almost double for some sensors compared to simulation. On animations (not shown) we observe a more homogeneous dispersion of the gas in the simulated case.

In the experiment, it seems that sensors 5 and 6 on the upper upstream part of the room are triggered first, then 7 in the upper middle place, then 1 and 3 (upper downstream) and finally 2 and 4 on the lower downstream part. In the simulation, the order of triggering is different: 2 and 4 first, followed by 1 and 3, then 7 and 8, and finally 5 and 6. We see that the light gas follows the flow path, which is different in the simulation and the experiment.

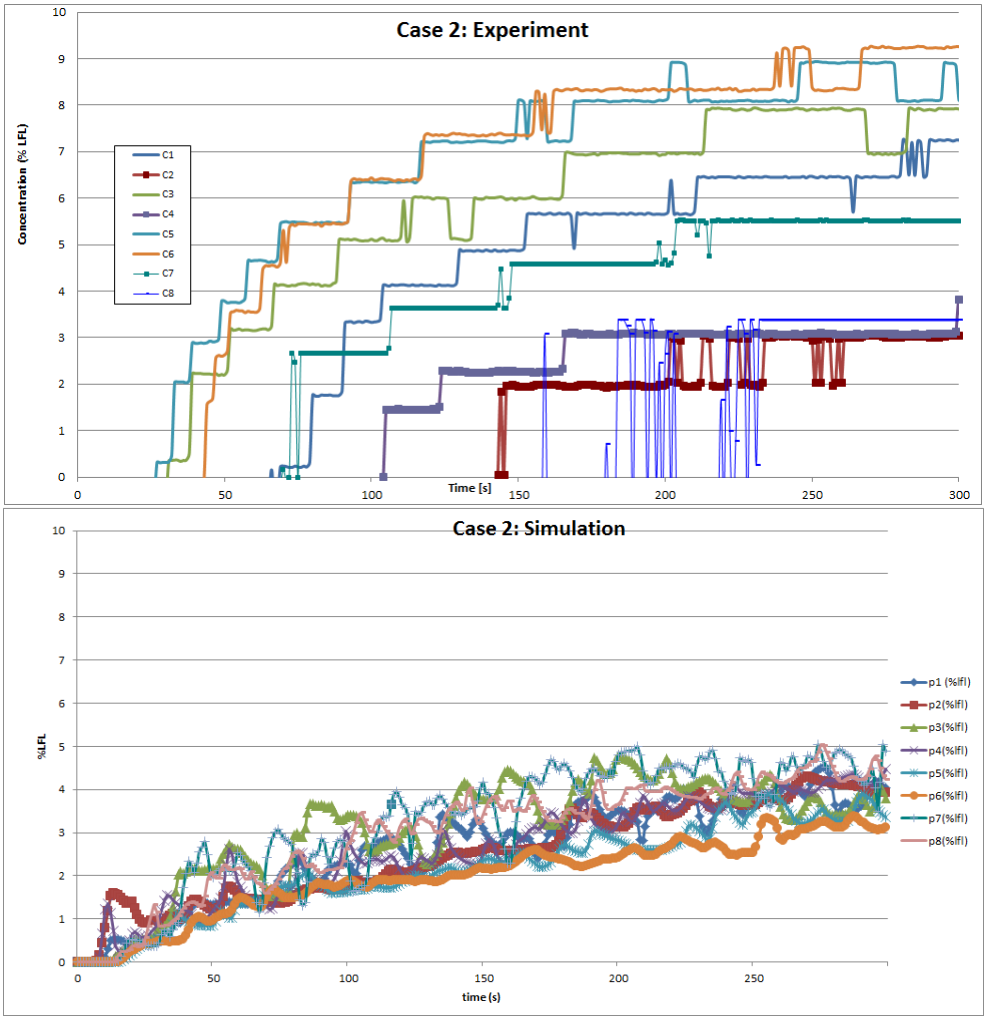

Figure 2.5 *Concentration as % LFL (lower flammable limit) against time (experiment top, simulation bottom).*

When we put the correct ventilation rates (2028 m^3/h corresponding to about 18 m/s extraction close to 8), the reason for this discrepancy may come from a false calculation of the jet itself, which interacts with the ventilation flow and divert the flow paths. The simulated velocity close to the exit shows high values, about 304 m/s and very high turbulent intensity (3000%), which is not realistic. From the discussion above, we expected anyway a max value of velocity close to 500 m/s. Both the high turbulent dissipation and the adiabatic expansion in Fluent may explain this difference. It could also be that the turbulent model k-ε-rng with pressure-based solver is not well suited for this highly compressible flow.

2.3.2 Results on case 4 (mixture of gas and droplets)

Figure 2.6 shows the concentration expressed in terms of percentage of the Lower Flammable Limit (LFL) of ammonia for case 4. In this case, we have treated the obstacle as an adiabatic wall (which is not correct for a stainless steel plate that was used in the experiment). Experimentally, the impinging droplets tend to cool the obstacle, and further maintain the liquid state of the next incoming droplets, resulting in about 15% rainout collected in the tray at 1 m distance from the nozzle. In the simulation, droplets do not form a film or/and rainout from the obstacle. The smaller droplets tend to follow the flow path. Most of the droplets will evaporate, so we do not expect much difference between simulated and observed gas concentration. The flow field was converged in about 10 s real time, and then frozen for the transport of temperature and concentration.

At first look at the ammonia vapour concentration data, the agreement seems good, although a slight underestimation (of about 15%) by the simulation is observed. Even the order in which the sensors are triggered seems satisfying. But it appears that we introduced a wrong over-pressure in the simulation set-up (pressure gauge of 2 bars instead of 1 bar from atmospheric pressure), tending to increase artificially the flow field (compensating in some way the much too high turbulence levels).

Figure 2.7 shows the concentration levels with the correct input values for pressure gauge and total temperature in the compressible inlet boundary condition. The simulations then underestimate the experimental results even more (a factor of 3 worse)! We still see the higher values for bottom sensors 2 and 4, logically as we have dense gas mixture effect (because of the cooling of the air from the evaporation process).

Figure 2.8 shows the temperatures in the experiment and the simulation. For the “erroneous” case, a much bigger temperature drop than in experiment is seen (almost 30 $^\circ C$ in the simulation, compared to the experimental values of 12 $^\circ C$ for sensors 2 and 4 on the bottom downstream and 15 $^\circ C$ and $^\circ C$ K respectively for the others). This discrepancy may come from a more efficient warming from surrounding air in the experiment in the entrainment phase, although the evaporation rates would be similar (almost the same vapour concentration levels are observed in the simulation and the experiment). The “corrected” results, see figure 2.9, have less differences for the temperature drop between the simulation and experiment (exception for sensor 7), but since the concentration results are not good for this case these may not be trusted.

When we look at the velocity value at the pipe exit, Fluent recalculate it from the fixed value 1.73 m/s and find about 400 m/s (we recall the theoretical value would be 89 m/s, less than sound

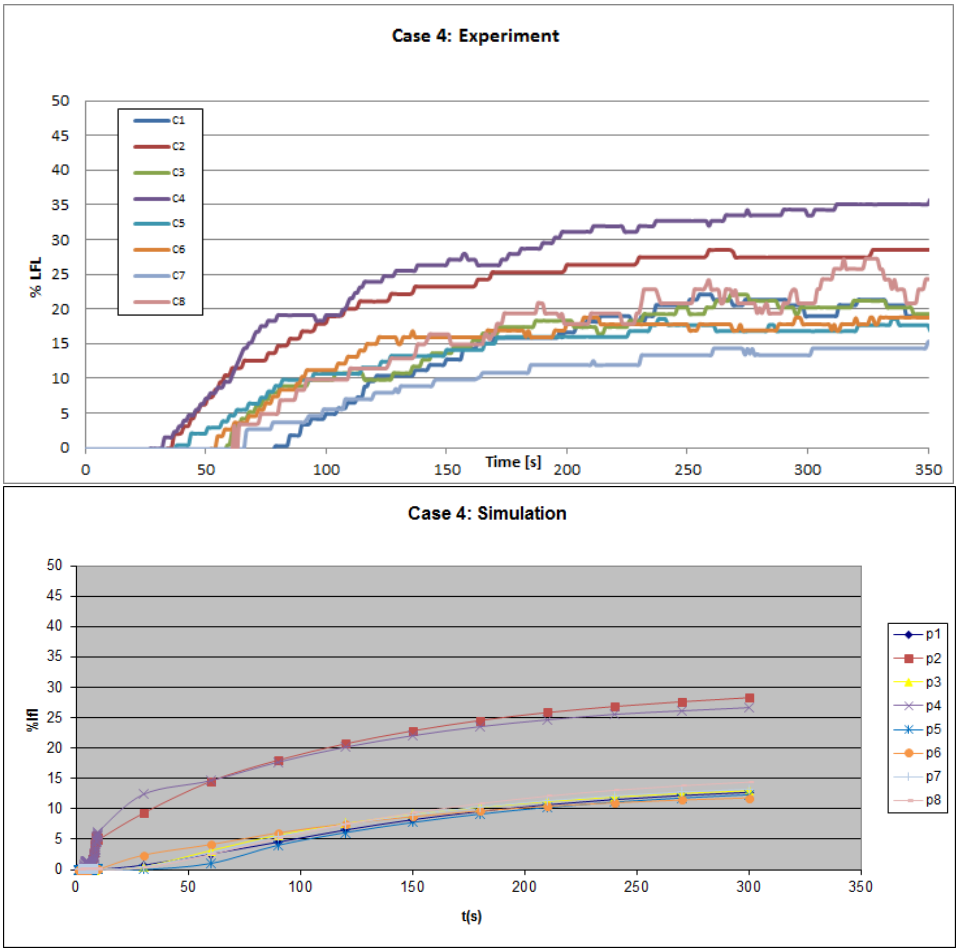

Figure 2.6 *Concentration as % LFL (lower flammable limit) against time (experiment top, simulation bottom).*

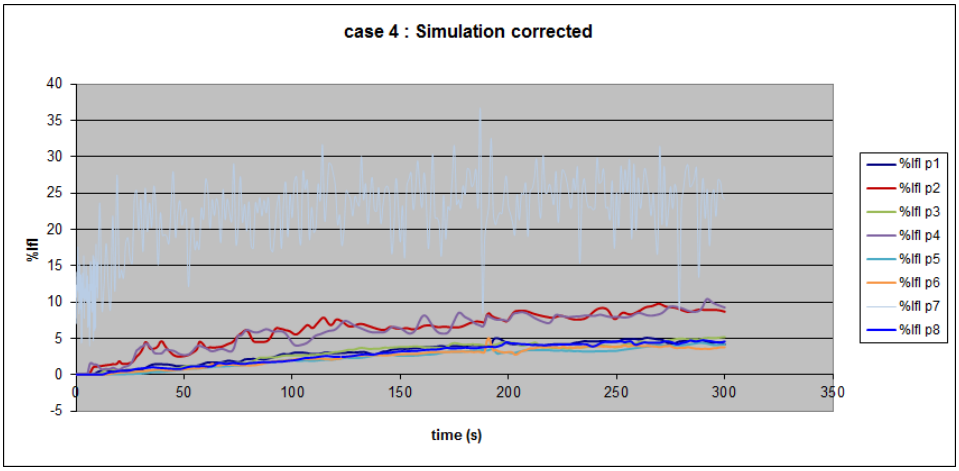

Figure 2.7 *Concentration simulated with the right over-pressure.*

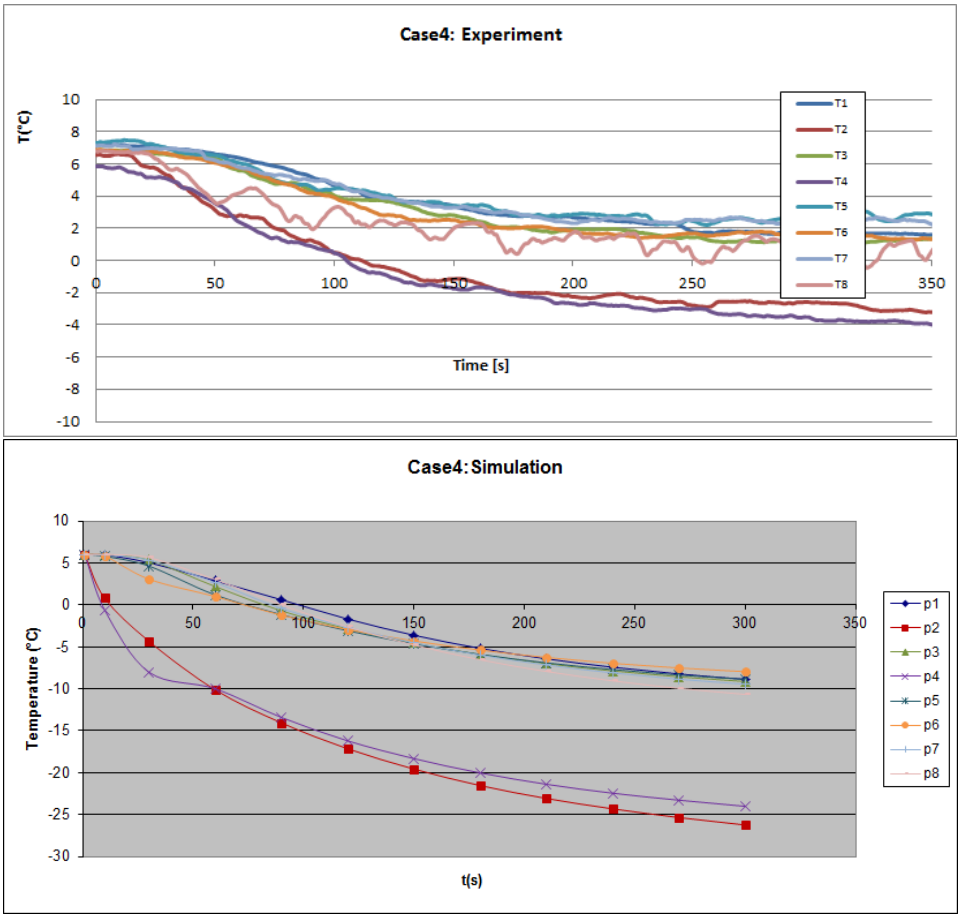

Figure 2.8 *Temperature drop against time (experiment on top, simulation on bottom).*

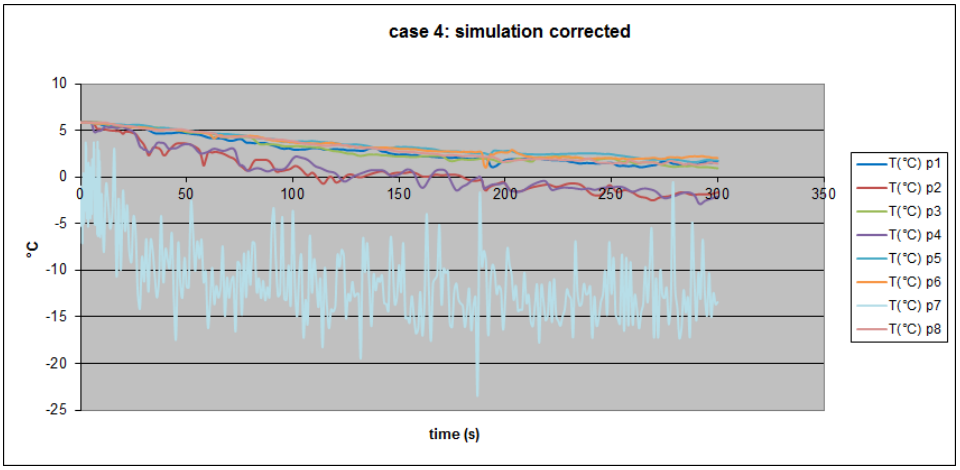

Figure 2.9 *Temperature drop against time for the simulation with the correct over-pressure (as in figure 2.7).*

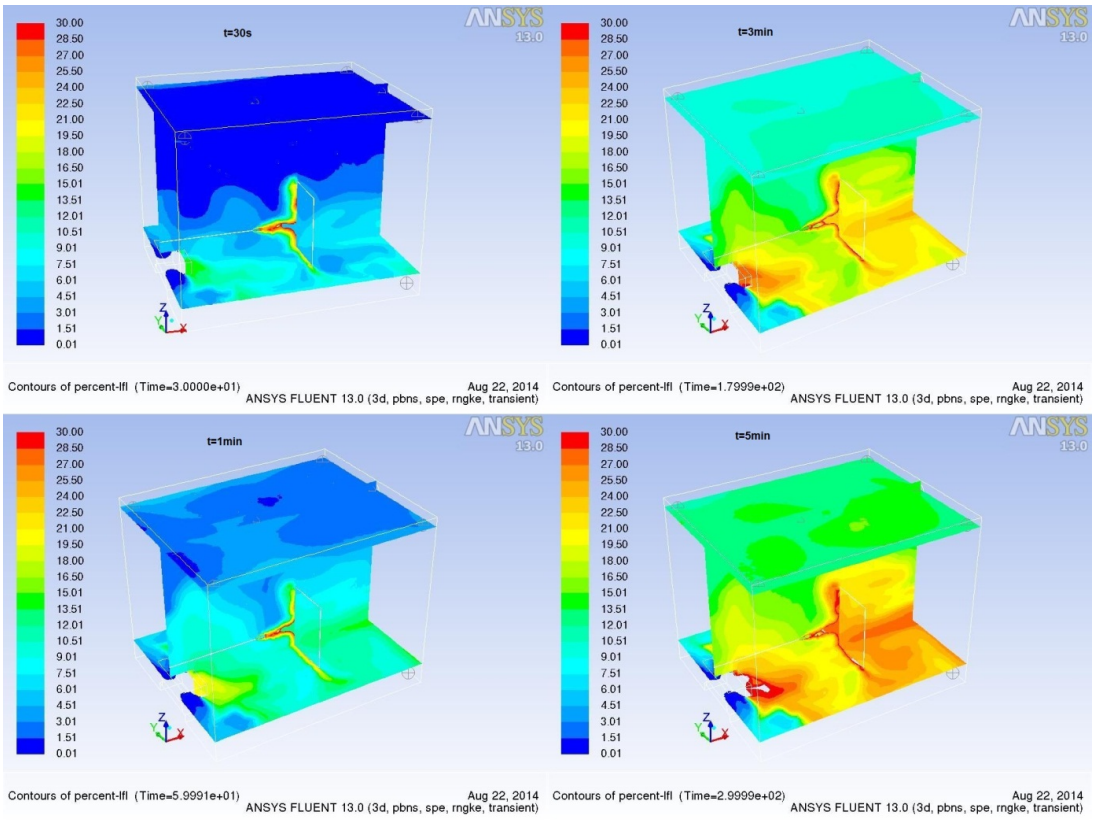

Figure 2.10 *Isocontours of the concentration field (%lfl) at times 30 s, 1 min (left), 3 min, 5 min (right).*

velocity at exit temperature). We obtain again a very high turbulent intensity >100%. The exit temperature is also unphysical (about 360 $°C$). These values drop very fast, over one diameter to respectively 100 m/s and 25 $°C$, which are quite reasonable.

In the Figure 2.10, we see at different time steps (30 s, 1 min, 3 min, 5 min) the % LFL in the "erroneous" case (which gave somewhat good results). We notice the dense gas is not efficiently dispersed and mixed with air, resulting in an over-concentration near the floor and behind the obstacle. The "corrected" case (bad correlation with results) in Figure 2.11 shows a much more homogeneous concentration field (this figure shows the mole fraction instead of % LFL).

We see in Figure 2.12 that the droplet concentration is limited to the jet region (although we truncated to 10^{-6} kg/m^3); almost all droplets evaporated before reaching the obstacle at 1 m.

The temperature at the exit of -16 $°C$ is lowered slightly by evaporation, but the mixing with ambient air increases the temperature quickly again (see Figure 2.13).

To complete the description, we show the turbulent intensity levels (truncated to 100 %) in figure 2.14 and the mean velocity levels in figure 2.15. It would of course be valuable to have experimental data for these variables for validation of the numerical procedure.

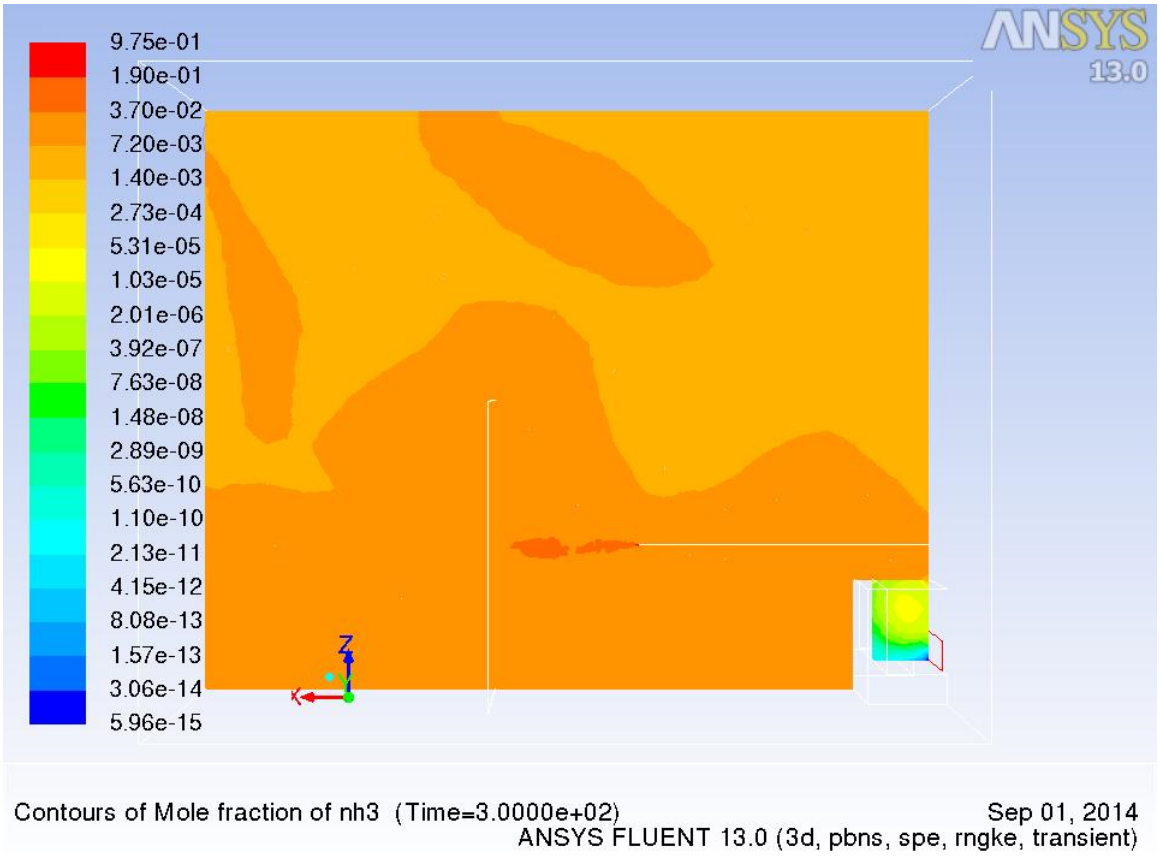

Figure 2.11 *Isocontours of the mass fraction in the symmetry plane at 5 min for the corrected case.*

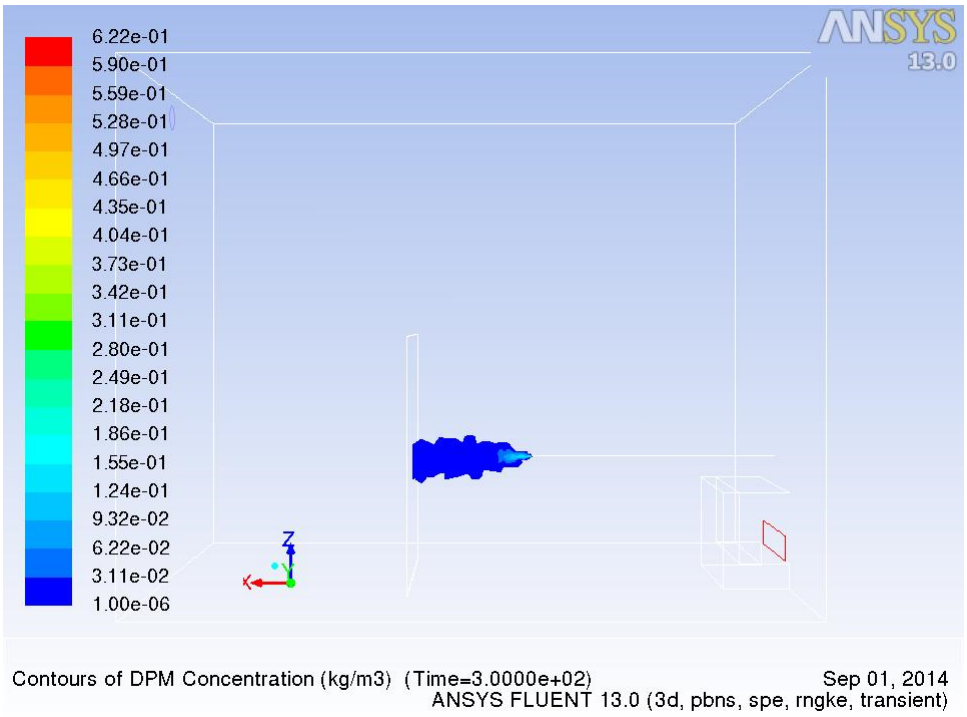

Figure 2.12 *Isocontours of the liquid droplet concentration in the symmetry plane at 5 min.*

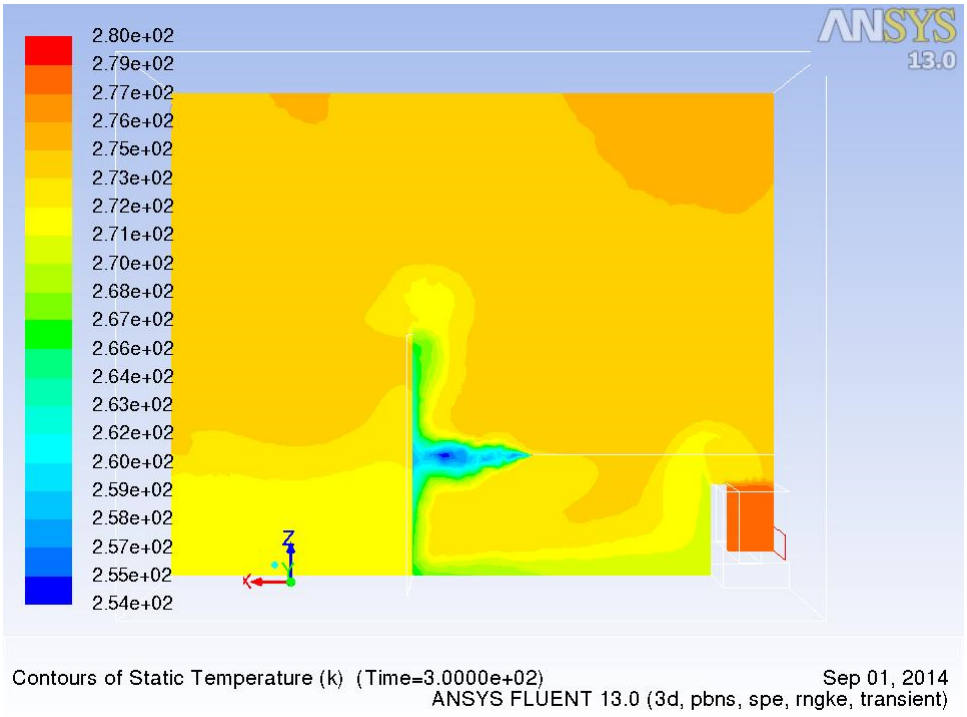

Figure 2.13 *Isocontours of the temperature in the symmetry plane at 5 min.*

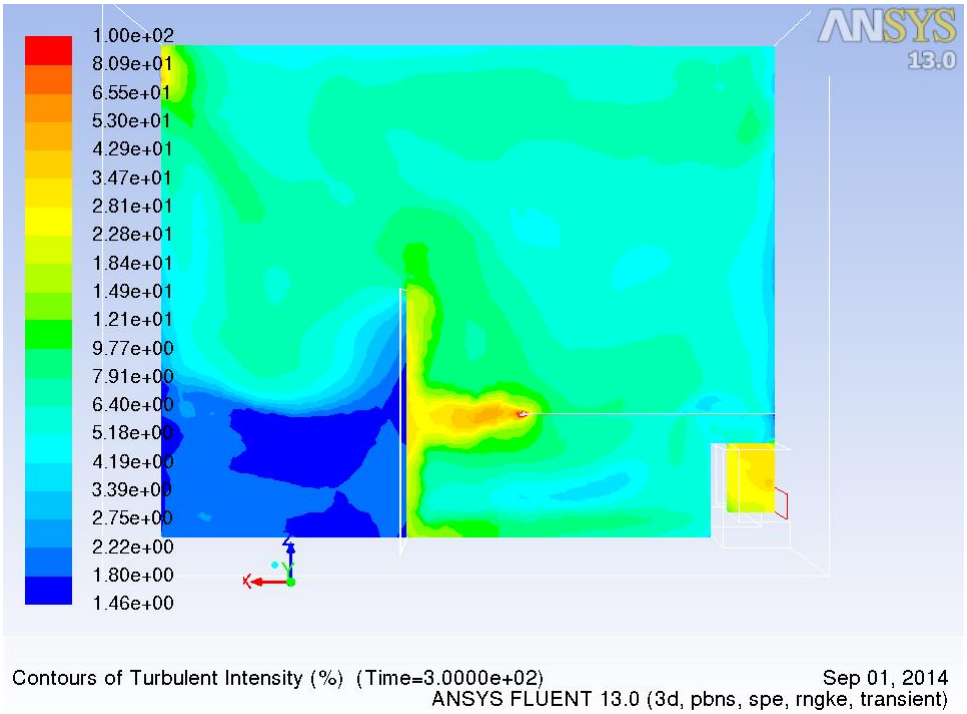

Figure 2.14 *Isocontours of the turbulent intensity in the symmetry plane at 5 min.*

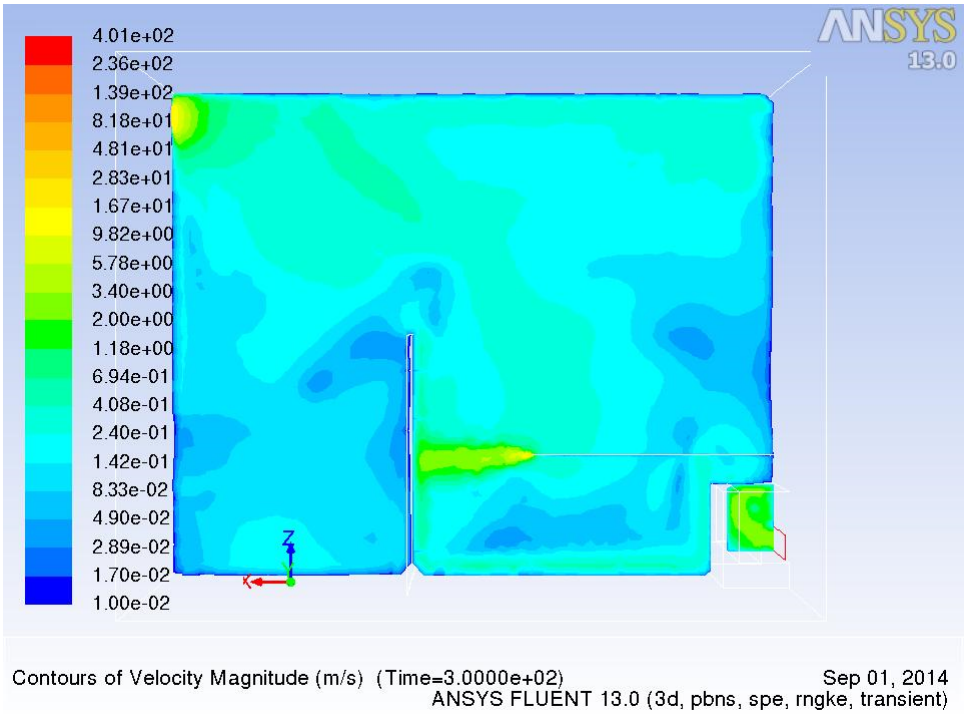

Figure 2.15 *Isocontours of the mean velocity in the symmetry plane at 5 min.*

2.4 Discussion

We can conclude that this attempt to simulate the dense gas release of pressurized liquid ammonia is not so promising for several reasons:

- Simulating the compressible gas accelerated due to the liquid phase flashing and expanding in surrounding air requires very small time steps (ms), which may be a strong constraint in larger domains
- The use of a pressure based solver instead of a density based helped converging the flow equations, but resulted in unrealistic values at the pipe exit, over-estimating the energy and turbulence well above admissible values (although results a few pipe diameters ahead where reasonable)
- The turbulence model k-ε-rng may not be suitable for highly unsteady and compressible gas flow, although usually well accepted for jet release impacting on obstacle.
- High sensitivity to geometrical details indoor and lack of experimental flow field data for these cases make the model validation difficult.
- The evaporation process seems well captured by mass and energy transfer between droplet phase and gas mixture, although we over-estimated the temperature drop in the room; this may come from a less efficient warm air entrainment, not well captured by RANS turbulence model.

The heat transfer to the obstacle was not considered here, but may delay the evaporation process by rainout of part of the liquid (about 15% in the experiment with the two-phase jet). Nevertheless, the concentration simulation results are within a factor of two of the observed data. We suggest to start the simulation at the end of the expansion phase, when the Mach number becomes small (<0.1). The difficulty would be to characterize the droplet distribution at that location, as well as the temperature and velocity field. This information may come from LES simulations on the first millisecond of the jet release, taking into account the whole process of fragmentation and mixing of gas and liquid.

3 FFI – LES modelling of indoor ammonia releases

The variable density solver vida, developed by Cascade Technologies, USA, has been used by FFI for simulating chlorine dispersion in the Jack Rabbit field trials [15]. It was therefore interesting to apply this method for modelling the indoor INERIS ammonia releases. However, it was not possible to reproduce the ammonia experiments. Here we describe the simulation strategies for the two cases and show why this effort could not reproduce the experiments.

3.1 Case 2 - pure gas release

For the single phase jet, the jet velocity is 172 m/s at the pipe outlet and it will increase further, resulting in a velocity at the end of the expansion region above the speed of sound (in ammonia) (see section 2.2.1). Because of this, it will not be possible to use "vida", as this is a low-Mach solver and will fail at such large velocities. Instead a compressible LES solver, charles, also developed by Cascade Technologies, was tested. This is a density based solver which uses the ideal gas law for the equation-of-state, and the VREMAN scheme for subgridscale modeling.

Figure 3.1 shows the geometry and mesh. Figure 3.2 shows the jet velocity after 0.03 s of release. The velocity in the simulation is overestimated, but the high velocity is extremely close to the outlet plane for the simulation. After just 1 mm the streamwise velocity has dropped to about 500 m/s.

One limitation with this model, is that it is not possible to include several substances. In other words it is not possible to release ammonia into air. This makes it difficult to find good starting conditions: it is not possible to get both the temperature and pressure set to the experimental values before the release. This is due to the fact that the initial ambient pressure and temperature in the experiment are that of air, but since only ammonia is included in the simulation, the gas law, using the molecular weight of ammonia, cannot produce both the temperature and pressure of air.

The model is developed for aeroacoustic applications; it is likely that there is some parameterization for that application in the code, and it is therefore not really valid for dispersion studies. In addition, running this code is extremely time consuming. A second of release took more than a week to simulate, so to simulate the entire experimental duration of 500 seconds is not feasible. Because of this, it is concluded that charles at present is not suitable for this problem. It is possible to alter the software to take several substances into account, but this requires some programming and changes to the software.

3.2 Case 4 - two-phase release

For this experiment, the semi-compressible LES solver vida was tested. FFI has used this code to simulate the dispersion of chlorine for the Jack Rabbit field trials [15].

Vida can be coupled to a Lagrangian spray model for liquid droplets. There is a two-way coupling between the gas phase and the liquid droplets for mass and momentum, so evaporating

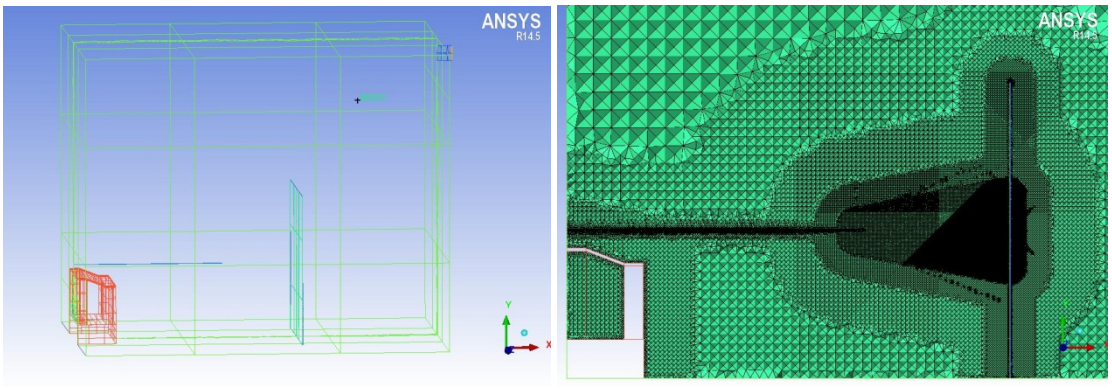

Figure 3.1 *The computational geometrical model including the deflector for the air inlet, the pipe for the chemical release, the obstacle and outlet pipe (left) and the computational mesh in a vertical slice through the geometry (right). The smallest cells at the pipe outlet is of the order of one mm).*

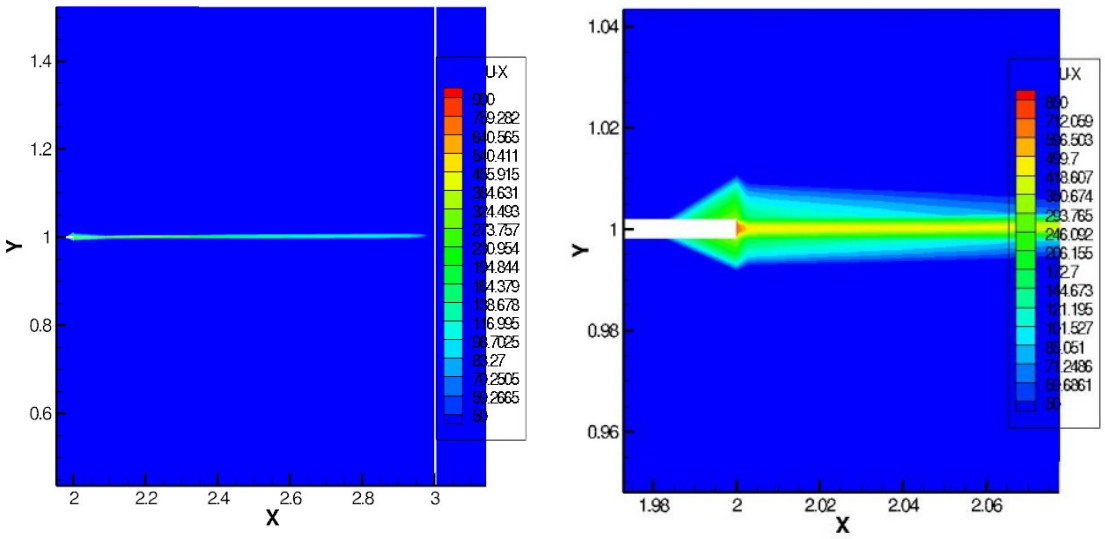

Figure 3.2 *The streamwise velocity component in a vertical plane along the direction of the release jet after 0.03 s. The two figures show the same instance in time, but the figure on the right is zoomed in on the jet exit.*

droplets constitute a source for vapour, and condensation should also be possible to simulate. However, there is only a one-way coupling for the temperature; the discrete phase model reads the gas temperature and uses that for calculating the evaporation, but evaporation does not affect the gas temperate. For chlorine this is not so critical, because chlorine is heavier than air anyway, but for ammonia the cooling of air by the evaporation process has to be taken into account to get the initial dense gas effects with ammonia liquid releases. Furthermore, vida does not solve the energy equation explicitly, instead a scalar transport equation is solved for the temperature. The vida code is developed for combustion studies, and the treatment of temperature and energy is parametrised for this application. Because of this, at the present time, the vida code is not applicable for the indoor ammonia two-phase experiment.

4 FOI – Modelling of the jet

4.1 Introduction

FOI has investigated and modeled the jet phase (following the release from a pressurized tank) in such a way that it is compatible with models and systems already developed at FOI. The basic physics is presented together with a verification section that includes data from experiments conducted by external organizations.

This work is the first part of two describing the modeling of dense gases by means of Lagrangian dispersion models at FOI. The second part of the Lagrangian dense gas modelling is described in [8].

4.2 Model description

A physical model has here been developed that aims to model a jet source for superheated liquid which is compatible with the dispersion models normally utilized by FOI. The goal with this source model is to provide a source term to the dispersion models where the inner processes and states of the jet are included but not necessarily expressed explicitly. Figure 4.1 shows a schematic illustration of the jet model.

The first process is a flashing of the liquid. This means that superheated liquid will immediately vaporize using the excess thermal energy until the released substance is a two-phase mix with one part liquid and one part vapor, all with the boiling temperature at atmospheric pressure. A gradual vaporization of the remaining liquid will thereafter take place as surrounding air is mixed in and thereby supplies the necessary thermal heat. Another effect of the entrainment of surrounding air is a decline in the velocity of the jet due to the conservation of momentum. The gas mixture will finally reach a state when all liquid has vaporized and the velocity is low enough to continue the simulation using dispersion models that supports dense gases. It is at this point that the jet model generates a suitable source model for FOI's dispersion model which is illustrated as a sphere in Figure 4.1. In this model it is assumed that any form of rainout is negligible, e.g., there will be no mass loss due to formation of liquid pools on the ground below the jet. This assumption has been found to be valid for jets consistent of superheated liquid that does not collide with any solid items [2]. The energy contribution from the condensation of water vapor and the loss of kinetic energy is also included where the first term is the dominating. The temperature of the final gas mixture will normally be substantially lower than that of the surrounding air which will result in a superior density of the gas mixture which therefore is described as a dense gas with properties that the subsequent dispersion models needs to address accordingly.

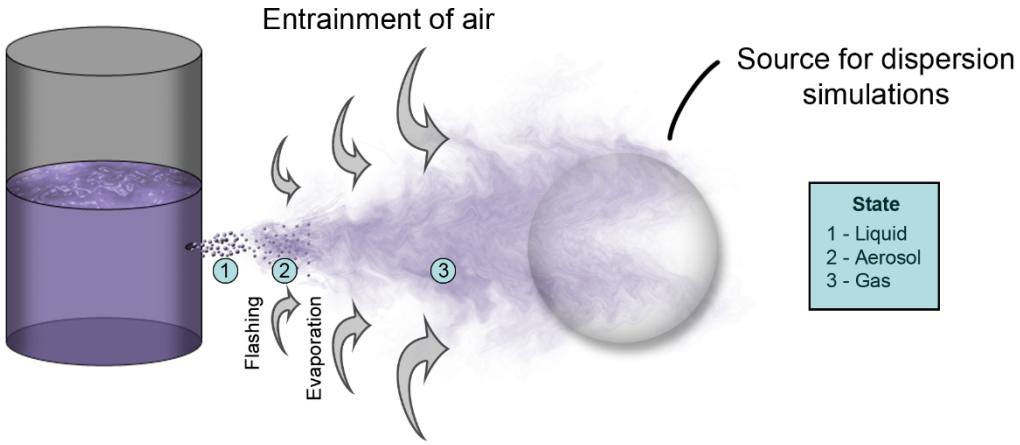

Figure 4.1 *Illustration of the source model. A minor hole in the container below the surface level of the fluid will give rise to a jet that undergoes three main processes: flashing, evaporation and air entrainment. The release of liquefied gas results in a jet that finally reaches a state where it is compatible with subsequent dispersion models.*

Assumptions for the model:

- The liquid in the jet may be modeled as if it is immediately vaporized. There will be no aerosols left and no rainout.
- When the liquid has vaporized, it will undergo an adiabatic expansion. An adiabatic process is here motivated by the fast time scale which means that any heat exchange with the surrounding air is negligible (partially due to the low thermal conductivity of air) and the fact that the surrounding air acts as a resistance when the gas expands.
- Both the air and the released gas can be described as ideal gases.
- The temperature and pressure of the container can be considered constant during the entire process.

Limiations of the model:

- The model does not include any effects of the size of the hole on the container regarding the jet angle. However, the model does include the effect the size of the hole has on the flow.
- The jet is assumed to take a conical shape and there is no influence from the ground or objects.
- The model does not take the surrounding wind speed into account.
- The model has no explicit support to simulate the pressure drop caused by a release through long hoses. Although, the coefficient C_d, which describes the characteristics of the hole, can be altered to manually compensate for this effect.

The process is modeled according to the following scheme of events:

1. Liquid is sprayed under high pressure and evaporates in two steps.
   (a) The superheated liquid partly evaporates where the heat of vaporization originates from the excess thermal energy of the liquid itself. This process continues until both the remaining liquid and the vaporized gas have a temperature that equals the boiling temperature at atmospheric pressure.
   (b) The remaining liquid evaporates, where the heat of vaporization originates from the entrainment air. The temperature of the gas now equals the boiling temperature at atmospheric pressure and the pressure equals the vaporization pressure at this temperature.
2. The gas expands adiabatically, *i.e.*, without any exchange of heat with the surroundings. The expansion causes the gas to conduct a work on the surrounding air which results in a temperature drop in the gas often substantially below the boiling temperature.
3. The kinetic energy is transformed into thermal energy in the entrainment air.
4. The water vapor in the entrainment air is condensed which adds thermal energy to the air.
5. During the process in the jet there is a constant entrainment of air from the surroundings which results in a mix of air and the released gas.
6. The air and the gas acquire a mutual temperature through heat exchange which means that heat is transferred from the entrainment air to the gas.
7. The final density of the gas mixture is derived from the temperature and equilibrium of the jet pressure with the surroundings.
8. The distance from the point of release is calculated based on the final ratio of densities between the gas and the air.
9. The expansion process is concluded and dispersion modeling of the final gas mixture of air and gas begins as dense gas modeling since the low temperature normally causes the gas mixture to have a density higher than the surrounding air.

This is also shown schematically in figure 4.2.

The word “gas” refers in this report to the vaporized gas, i.e., the released substance in gaseous form. The jet consists of a mixture of this gas and air. Index G represents the released gas and the index A represents the entrainment air. The index AG refers to both the air and the gas. Note that the state numbers indicated in Figure 4.2 are used as sub-indices to variables throughout chapter 4 to determine which state the variable refers to.

4.2.1 Thermodynamics

The physics used in the model are presented here.

4.2.1.1 Basic concepts

The ideal gas law

A basic relation within thermodynamics for non-reactive gases at low pressures is the ideal gas

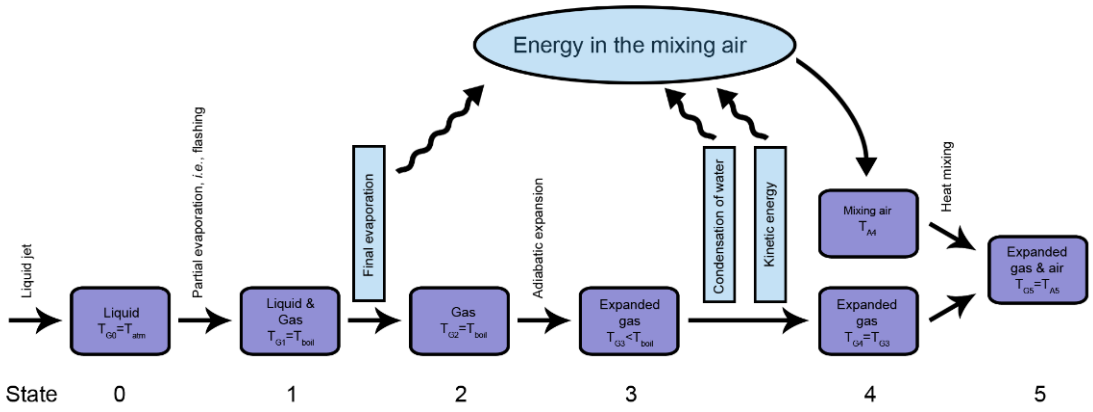

Figure 4.2 *Schematic presentation of the process in this model of a jet source for a dense gas release.*

law which is a state equation that describes the linear relation between pressure, P, volume, V, number of moles, n, and the temperature, T, using the universal gas constant $R = 8.31$ J/mol/K:

$$PV = nRT \tag{4.1}$$

The relation between the number of moles, n, the molar mass, M, and the mass, m, is

$$m = Mn \tag{4.2}$$

Equation 4.1 can be written

$$P_{AG_i} = \frac{RT_{AG_i}}{V}\frac{m_{AG_i}}{M_{AG}} = \frac{RT_{AG_i}\rho_{AG_i}}{M_{AG}} \tag{4.3}$$

for the gas in the volume V where ρ is the density.

Dalton's law

Dalton's law states that the total pressure of two mixed gases equals the sum of their partial pressures which in this case means that the sum of the partial pressures for the gas and air approximately equals the surrounding atmospheric pressure at the final state of the jet.

$$P_{atm} = P_G + P_A \tag{4.4}$$

4.2.1.2 Partial evaporation

The released fluid is superheated which means that the temperature is higher than the boiling temperature at the surrounding pressure (here atmospheric pressure). This implies a rapid and violent evaporation, so-called flash, of one part of the fluid where the enthalpy of vaporization

lowers the temperature in the liquid and in the gas down to the boiling temperature. The fraction of the liquid that evaporates by means of flashing is

$$X = (T_0 - T_{G,boil}) \frac{C_p}{h_G} \tag{4.5}$$

where T_0 is the original temperature of the liquid, $T_{G,boil}$ is the boiling temperature for the liquid at atmospheric pressure, C_p is the heat capacity of the fluid and h_G is the enthalpy of vaporization for the substance. The remaining liquid evaporates within the jet and the energy for this process is assigns to the entrainment air and will reappear later in the process. In this state, number 2 in Figure 4.2, the temperature equals the boiling temperature: $T_{G_2} = T_{G,boil}$.

4.2.1.3 Adiabatic expansion

When the liquid undergoes a phase transition into gaseous form, the local pressure increases which leads to an expansion until equilibrium in pressure is obtained. This thermodynamical process is best described as an adiabatic process since the system is thermally isolated, *i.e.*, there is no transfer of heat between the expanding gas and the surrounding medium. Two different methods that describe an adiabatic process of expanding gas is presented below, where the second method is implemented in this jet model.

The energy that is lost by the work conducted on the surrounding air is not stored locally but rather transported through the medium and will not reappear anywhere in the model.

Dropping pressure

In this method it is assumed that a package with gas is instantaneously created carrying its vapor pressure, which then drops as the package is expanding. The temperature subsides with the pressure. Equation 4.6 is valid for an adiabatic expansion of ideal gas

$$P^{1-\gamma} T^{\gamma} = constant \tag{4.6}$$

where γ is the relation between the specific heat capacity at constant pressure and constant volume, respectively [16]. This parameter depends only on the molecular structure of the gas and can be written as

$$\gamma = \frac{\alpha + 1}{\alpha} \tag{4.7}$$

where α is the number of degrees of freedom of the molecule divided by two. This implies that $\gamma = 5/3$ for monoatomic gases and $\gamma = 7/5$ for diatomic gases. Air is a mixture of different substances but is heavily dominated by N_2 and O_2 which both are diatomic. For the adiabatic expansion in the jet, equation 4.6 can be written as

$$T_{G_3} = T_{G_2} \left(\frac{P_{G_2}}{P_{G_3}} \right)^{\frac{1-\gamma}{\gamma}} \tag{4.8}$$

where P_{G_2} is the pressure of the released gas after evaporation but before the expansion takes place, *i.e.* the vapor pressure which often is the current pressure inside the container. At this moment, state 2 in Figure 4.2, the temperature of the gas equals the boiling temperature, $T_{G_2} = T_{G,boil}$.

Constant pressure

When the liquid evaporates, gas is created with higher pressure than the surroundings leading to an expansion until equilibrium in pressure is obtained. This process can be assumed to take place at the speed of sound whereby there is not enough time to build up high pressures. In this method it is assumed that the pressure of the gas is negligibly higher than that of the surroundings during the process, *i.e.*, the expansion of the gas is a quasistatic process at atmospheric pressure. The work that the gas conducts on the surroundings during the expansion is

$$dw = P_{atm} dV \tag{4.9}$$

which means that the total work per unit of mass becomes

$$w = P_{atm} \left(\frac{1}{\rho_G} - \frac{1}{\rho_L} \right) \tag{4.10}$$

where ρ_G and ρ_L are the densities in gas and liquid form, respectively [3]. This expansion cools the gas itself down to the temperature T_{G_3}

$$T_{G_3} = T_{G_2} \frac{1}{\frac{R}{MC_p} + 1} \tag{4.11}$$

Here it has been assumed that $\rho_L >> \rho_G$ and ρ_G is calculated using equation 4.3 at atmospheric pressure.

4.2.1.4 Energy exchange with the entrainment air

There are three processes involved in the energy exchange with the entrainment air: evaporation of the gas (e_{Avd}), condensation of water vapor (e_{Con}), and loss of kinetic energy (e_{Kin}). The evaporation is a negative contribution since heat is taken from the entrainment air to evaporate the fraction of the liquid that does not flash. Condensation of the water vapor leads to a positive contribution as is the case with the loss of kinetic energy. The last factor is normally negligible in this process. Calculations is performed using intensive properties. The entity e, which is the energy density ($\left[\mathrm{J/m^3}\right]$), is used. The contribution from evaporation to the entrainment air is

$$e_{Avd} = -h_G \rho_{G_4} (1 - X) \tag{4.12}$$

where h_G is the enthalpy of vaporization for the gas. Condensation of water vapor implicates that the latent heat is added to the entrainment air.

$$e_{Con} = h_{H_2O} \frac{\rho_{A_4}}{\rho_{atm}} \rho_{H_2O_{Max}} \Phi \tag{4.13}$$

where Φ is the relative humidity and $\rho_{H_2O_{Max}}$ is the maximum density of water vapor in the air under current meteorological circumstances. The factor ρ_{A_4}/ρ_{Atm} compensates for the fact that the volume is not entirely occupied by air. By neglecting the small amount of kinetic energy left in the jet at the final state, the energy contribution from the loss of kinetic energy density for the gas can be written as

$$e_{Kin} \approx \frac{u_{G_1}^2}{2} \rho_{G_4} \tag{4.14}$$

The energy density added to the entrainment air is summed up as

$$e = e_{Avd} + e_{Con} + e_{Kin} \tag{4.15}$$

The temperature of the entrainment air then becomes

$$T_{A_4} = T_{A_3} + \frac{e}{\rho_{A_4} C_{p_A}} \tag{4.16}$$

4.2.1.5 Temperature equalization

The temperatures T_{G_4} and T_{A_4} represent the temperatures of the gas and the air, respectively, before they have undergone a heat exchange and thereby obtained the new common temperature T_5 that lies between T_{G_4} and T_{A_4}

$$T_5 = T_{G_4} + \frac{c_{P_A}\left(T_{A_4} - T_{G_4}\right)}{c_{P_A} + c_{P_G}\frac{Y_b}{1-Y_b}} = T_{G_4} + \frac{T_{A_4} - T_{G_4}}{1 + \frac{c_{P_G}}{c_{P_A}}\frac{\rho_{G_4}}{\rho_{A_4}}} \tag{4.17}$$

where c_{P_G} and c_{P_A} are the thermal capacities for the gas and the air under constant pressure, respectively, and

$$\rho_{A_4} = \rho_{G_4}\frac{1 - Y_b}{Y_b} \tag{4.18}$$

where Y_b represents the fraction gas in the mixture according to

$$Y_b = \frac{m_G}{m_a + m_G} = \frac{\rho_G}{\rho_A + \rho_G} \tag{4.19}$$

4.2.2 The jet

The description of the jet is mainly based on chapter 6 in [17].

4.2.2.1 Outflow

The velocity of the outflow, u_e, can be calculated by the difference between the pressure in the container, P_0, and the atmospheric pressure P_{atm}

$$u_e = \sqrt{2\nu_f\left(P_0 - P_{atm}\right)} \tag{4.20}$$

where ν_f is the specific volume in the liquid [18]. The mass flow Q is given by

$$Q = C_d A\sqrt{\frac{2\left(P_0 - P_{atm}\right)}{\nu_f}} \tag{4.21}$$

where C_d is a constant that describes the characteristics of the edges of the hole with a value in the range 0–1 which can be estimated from the information in Table 4.1.

The momentum flux, F, in the jet is derived by multiplying the mass flow and the velocity of outflow.

$$F = Qu_e \tag{4.22}$$

C_d	**Description**
0.5	Punched hole from the outside
0.6	Sharp edges
0.95	Smooth edges

Table 4.1 *The value of C_d as function of the appearance of the hole.*

4.2.2.2 Entrainment

According to chapter 6.2.1 in [17] there is empirical data that support the following expression for the entrainment density q, *i.e.* the amount of entrainment air per length and time, in the jet.

$$q = \frac{\sqrt{\rho_a F}}{\chi} \tag{4.23}$$

where χ is a constant entrainment factor. The mean velocity of the jet, u, in the position x is formulated as

$$u = \chi \sqrt{\frac{F}{\rho_a}} \frac{1}{x} \tag{4.24}$$

The position is also coupled to the ration of the densities as

$$Y_b = \frac{\chi Q}{\sqrt{\rho_a F}} \frac{1}{x} \tag{4.25}$$

The jet has a certain angle of propagation, α, that describes how the width of the jet increases with distance from the release point. This parameter is constant which gives rise to conical shaped jet with a radius that can be written as

$$R = x \tan \alpha \tag{4.26}$$

4.2.2.3 Angle of propagation

A brief deduction of the relationship between the angle of propagation and the entrainment factor is given here. The entrainment rate is constant in all yz-planes along the propagation axes of the jet and is written

$$q = \frac{d\left(\rho u A\right)}{dx} = \rho \left(A \frac{du}{dx} + u \frac{dA}{dx} \right) \tag{4.27}$$

where A is the intersection area of the jet at the position and any variations in densities is assumed to be negligible.

$$\frac{dA}{dx} = \frac{2A}{x} \tag{4.28}$$

$$\frac{du}{dx} = -\frac{u}{x} \tag{4.29}$$

The equations 4.27-4.29 give

$$q = \rho \frac{Au}{x} \tag{4.30}$$

By using equations 4.23 and 4.30 the following equality is obtained

$$\frac{\sqrt{\rho_a F}}{\chi} = \rho \frac{\pi (\beta x)^2 \chi \sqrt{\frac{F}{\rho_a}} \frac{1}{x}}{x} \tag{4.31}$$

where β is the proportional factor between the radius and the position x, *i.e.*, $R = \beta x$. The density ρ rapidly approaches ρ_a which mean that they can be eliminated from the equation. Thereby, equation 4.31 can be rewritten as

$$\beta = \sqrt{\frac{1}{\chi^2 \pi}} \tag{4.32}$$

According to calculations by Fischer *et al.* [17] based on empirical data from Ricou et al. [19] and Hinze *et al.* [20], the angle of propagation is $\alpha = 9.2$ degrees for a uniformly distributed jet and $\alpha = 12.4$ for a non-uniformly distributed jet. The term distribution refers here to the distribution of gas concentration and temperature in the jet. Since the model presented here assumes uniformly distributed parameters during the jet phase an angle of propagation of $\alpha = 9.2$ degrees is implemented. A higher value on the entrainment factor results in a reduced injection of air and thereby a more narrow jet that will need a longer distance to reach its final conditions. The diameter of the plume, D, is thus

$$D = 0.32x \tag{4.33}$$

4.2.2.4 Final condition for the jet

As an addition to the thermodynamical equations, a condition that determines at which point the jet has reached it final state is required. Here, a final velocity, u_{end}, is used as this condition.

The equations 4.24 and 4.25 provide the following relation between the velocity of the jet and the density ratio

$$Y_b = u \frac{Q}{F} \tag{4.34}$$

Now, the final condition will imply that

$$Y_b = u_{end} \frac{Q}{F} \tag{4.35}$$

Bricard *et al.* [6] suggest that the final condition should be

$$u_{end} = 0.8 u_{atm} \tag{4.36}$$

This parameter is left as an input parameter in this model to provide the user with the possibility to obtain a custom source term that is suitable for different situations.

4.3 Verifications

The results from the model are here compared to two independent sets of experimental data from in this section.

The first data set is from the FLADIS-experiments conducted at Risø, Roskilde Denmark, in the 1990s with release of liquefied ammonia [10, 11]. The second data set is from the INERIS-experiments conducted at CEA-CESTA, Bordeaux, France during the period of 1996-2012 where also liquefied ammonia was used [9].

The jet model has not been adapted in any specific way towards these measurements with the exception of the parameter C_d which has been modified to give rise to a correct mass flow. The value of C_d that should be used depends on the nozzle, see Table 4.1. In the FLADIS case $C_d = 0.697$ was used while a significantly lower value was used in the INERIS case, $C_d = 0.177$. Both experiments utilized long pipes from the containers to the release nozzles which may give rise to significantly lower mass flows than what would have been the case with holes directly on the containers. To keep track of this, pressure sensors were mounted close to the orifice in both cases. In the FLADIS experiments the pressure at this point remains equal to the vapor pressure, *i.e.*, 7.98 bar, while in the INERIS experiments the pressure had dropped to approximately 2 bar. I the latter case a drop in temperature of almost 30 Kelvin over the release system was observed. The conclusion from these facts is that there was internal flash in the pipes in the INERIS experiments. Fischer *et al.* concludes that such a situation gives rise to a critical flow which results in a decreased mass flow [17]. To compensate for this phenomenon, a low value on C_d is needed in the jet model.

4.3.1 Angle of propagation

Figure 4.3 shows the functions for a normal and a circularly uniform distribution, respectively. The normal distribution corresponds to the specified jet size from test number 4 in the INERIS-data with the assumption that the jet is still symmetric in the yz-plane. The width is defined as the perpendicular distance from the center of the jet where the concentration amounts to half the value of the concentration at the center. At a distance of 20 meters the width is reported to be approximately 5 meters which implies that a corresponding normal distribution would have a standard deviation of 2.12 meters.

It is reasonable to assume that the jet is not quite as high as it is wide at a distance of 20 meters even though there are no data to support the claim. That is, the jet has started to spread horizontally as it has descended down to ground level. If this really is the case it would mean that the normal distribution shown in Figure 4.3 has a somewhat exaggerated variance in the two-dimensional plane. The green circular distribution depicts the jet models description of the same plume which always has a uniform distribution.

Note that the angle of propagation for the uniform distribution is based on data from other experimental data than the INERIS data. This comparison shows a good agreement in the angle of propagation which suggests that the value of $\alpha = 9.2$ degrees is applicable.

4.3.2 Temperature

A comparison between the jet model and temperature data from the FLADIS experiments is presented here. Figure 4.4 shows the experimental setup close to the source. A rig of thermocouples (type K) was placed at a distance of seven meters from the source.

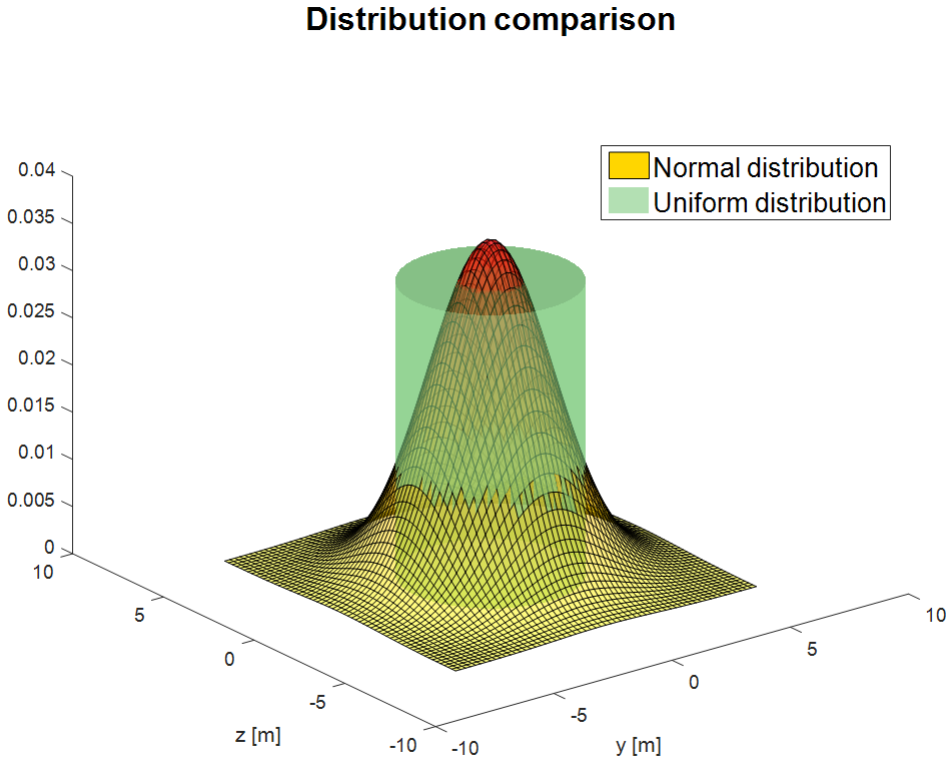

Figure 4.3 *A comparison between a uniform and a normal distribution. The normal distribution indicates the size of the jet at a distance of 20 meters in the INERIS data set (test 4) assuming that the jet still is conically shaped. The green cylinder indicates the corresponding size of the uniform distribution of the jet model with an angle of propagation of 9.2 degrees.*

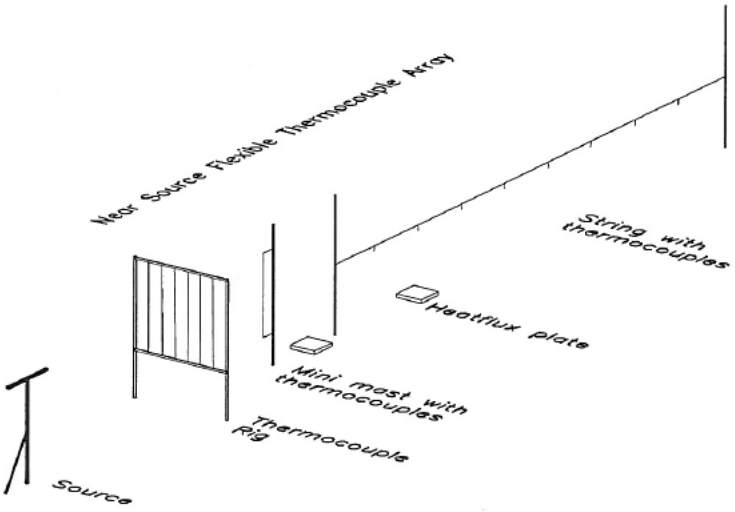

Figure 4.4 *The setup close to the source in the FLADIS- experiment. The experimental data of interest was obtained from the rig closest to the source (distance of 7 meters).*

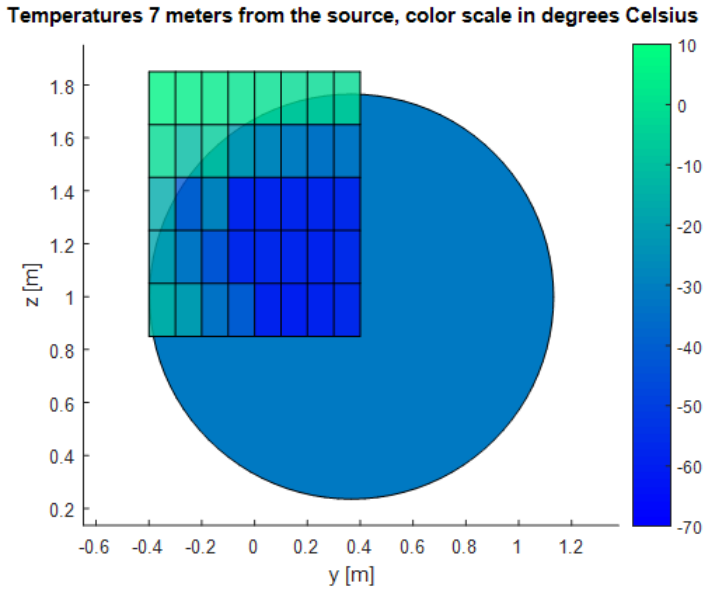

Figure 4.5 *A comparison between model data and FLADIS data illustrated with a color scale according to the temperature. The grid shows the time averaged measurement data from the rig while the blue circle shows the model size and temperature. The point of view is along the x-axis looking towards the source.*

The position of the jet from the model has been modified in the y-direction corresponding to 3 degrees due to the reported wind direction at the time of the experiment. Moreover, it has been lowered 0.5 meters in z-direction compared to the actual source height (at 1.5 meter) to better match the results since the jet is descending towards the ground in an unknown pace. Figure 4.5 shows data from the experiment (the rig) as well as the uniformly distributed temperature from the jet model (the circle). Unfortunately, a substantial fraction of the jet missed the rig in the experiment which complicates a detailed comparison. It is, however, possible to conclude from figure 4.5 that there is a descent agreement since the model's temperature is indeed between the lowest and the highest temperatures in the corresponding area. The time averaged mean of all measured temperatures on the rig in the experiment is -34 $^{\circ}C$ and the temperature of the model is -31 $^{\circ}C$.

Temperature measurements from the string of thermocouples at distances 11.25 to 18.25 meters could have provided important information. It seems, though, that the jet misses them too much for the data to be useful, see Figure 4.6. The thermocouples are positioned at the coordinates y=0.0 m and z=1.0 m which corresponds to a temperature colder than the model temperature at the grid. However, the string of thermocouples all measure temperatures close to the ambient air temperature indicating that the jet misses them almost entirely.

4.4 Input to and output from the jet model

The required input and the provided output of the jet model is listed below.

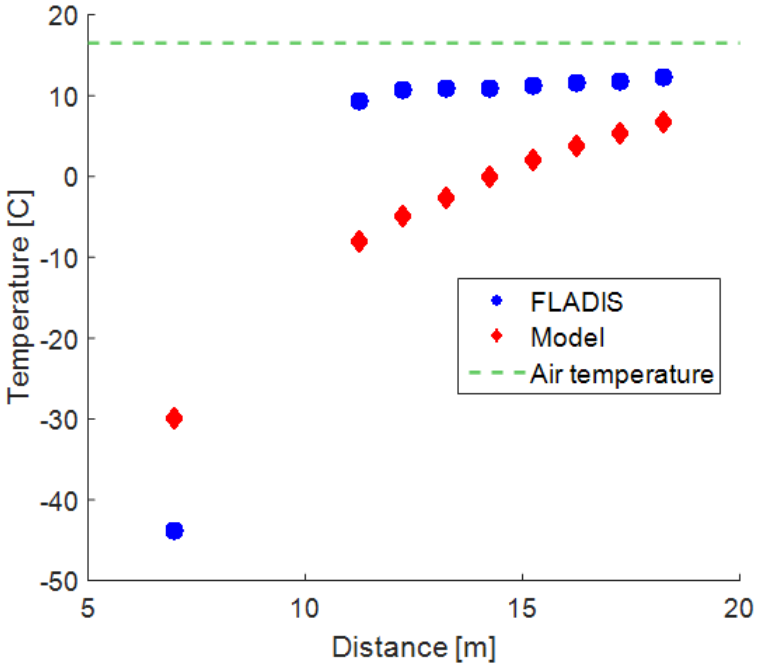

Figure 4.6 *Time averaged temperatures from the string of thermocouples (located at position y=0.0 m and z=1.0 m) as a function of distance from the source. The point at 7 meters is taken from the thermocouple closest in yz-position in the rig.*

Indata:

- Meteorological data
- Substance data, which can be imported from a catalogue of substances
- Release information
  - The size of the hole
  - The value on the dimensionless factor that described the flow resistance of the edges of the hole
  - The inner pressure at the nozzle which often equals the vapor pressure in the container
- The angle of propagation of the jet
- The velocity of the jet that acts as the final condition

Outdata:

- The cross-section area
- The distance from the release point
- The temperature
- The density of the mix of gas and air

4.5 Discussion

Many dependent and nonlinear processes take place at overlapping time intervals during the release of superheated liquid from a container. To describe them in detail is a complex task which has been attempted in both theoretical and numerical approaches with varying results. In this work the aim has been to describe the state of the jet when a certain final condition is fulfilled by means of thermodynamical relations. The model does not, by no means, claim to elucidate the intricate state of the two-phase flow at intermediate positions in the jet. However, the model does provide a dense gas source model suitable for further dispersion modeling. Comparison has been conducted towards the FLADIS-experiment and somewhat against the INERIS-experiment, although experimental data available for comparison is limited and more effort in the verification of the model would be profitable. The phenomenon included in the model are all selected from previous published models conducted by other actors which suggests that this model is in line with mainstream modeling of jets originated from superheated liquid from a physical point of view.

5 INERIS – LES modelling of outdoor ammonia releases

5.1 Introduction

This chapter focuses on the ability of the LES code FDS to model the release and transport of ammonia. Two steps are required for such an objective. The first is to demonstrate the ability of the FDS code to reproduce the experiments, the second is to build a methodology that is predictive. This chapter clearly focuses on the ability of the CFD code to reproduce experiments, that is to show the possibility of modelling a given experiment. One of the main difficulties is the need for detailed and reliable input data, considering using LES for atmospheric dispersion modelling requires building turbulence spectrum. Large scale INERIS ammonia releases were used in this paper mainly because it corresponds to a free field jet release that can be used to validate the CFD tools in predicting the consequences of toxic industrial chemicals (TICs) atmospheric dispersion following an accident. The main part of the chapter details the methodology built for evaluating the FDS capability to model such an experiment.

5.2 Modelling the INERIS ammonia fields experiment with FDS

Fire Dynamics Simulator (FDS) is a freely available CFD code developed by NIST[2] [21] to compute fires and smoke propagation. The turbulence model is based on the LES approach. Previously some LES simulations were published by Mouilleau *et al.* [22] based on a simple approach uncorrelated with experimental measurement or theoretical development. Such an approach enables to build a fluctuating velocity profile in the domain inlet. The simple approach developed in this work is an extension of this methodology to take into account the large variety of frequencies due to the large number of turbulent fluctuations. This approach is based on a Fourier analysis of an experimental profile.

5.2.1 Ammonia dispersion INERIS field tests

The ammonia dispersion field tests performed by INERIS [23] are briefly presented. In 1996 and 1997, INERIS conducted real-scale releases of ammonia in open air with the help of major sponsors. These tests were intended to reproduce as closely as possible an accidental scenario that may occur in a real industrial facility. Outdoor experiments were conducted on the testing site of CEA-CESTA (Centre of Scientific and Technical Studies of Aquitaine) that had a surface area of 950 ha and was completely flat. Figure 5.1 shows the whole measurement area in CEA-CESTA field.

During the experiments, the atmospheric conditions were determined using a meteorological mast which was installed 350 m from the release point (label “M” in Figure 5.1). This mast was 10 m high and was equipped with 3 cup anemometers located at 1.5, 4 and 7 m above the ground, a wind vane at 7 m and an ultrasonic anemometer at 10 m. A weather station was also installed

[2]National Institute of Standards and Technology, U.S.

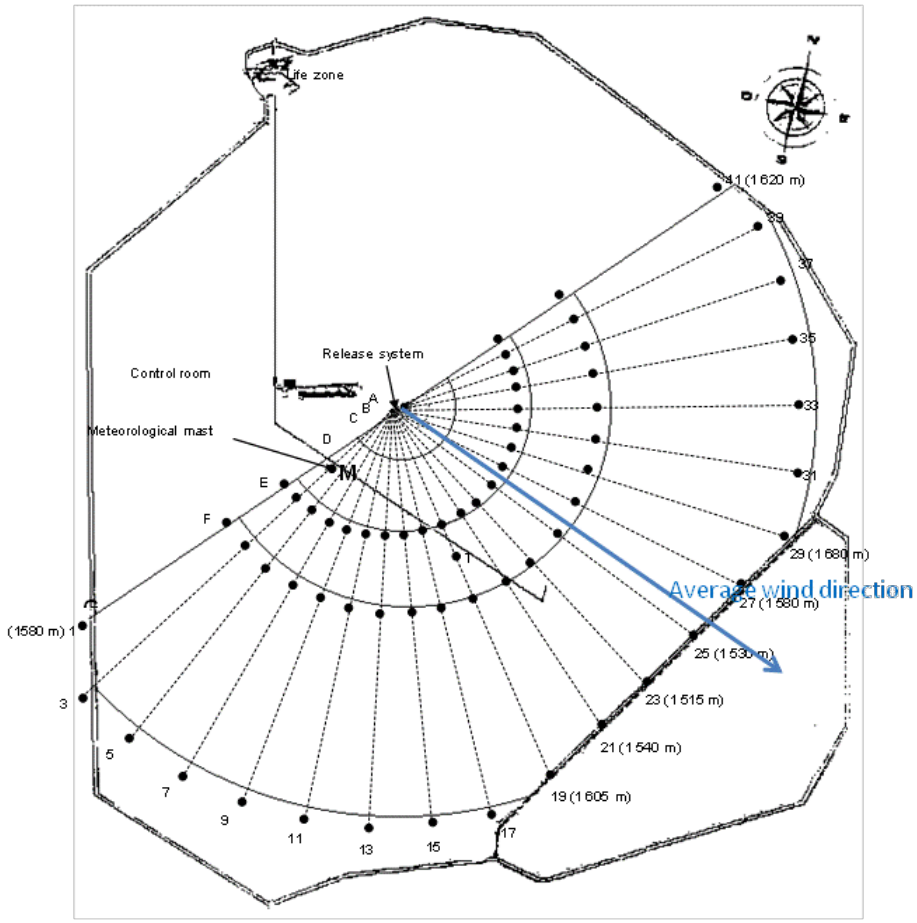

Figure 5.1 *The whole measurement area in CEA-CESTA for the ammonia experimental test cases; sensor arcs locations (distances from the release system : 20 m, 50 m, 100 m, 200 m, 500 m, 800 m and 1700 m for corresponding referenced letters A, B, C , D, E, F, G)*

Ambient temperature °C	Relative Humidity %	Solar Flux (kW/m2)	wind speed at 7 m (m/s)	Pasquill Class
12.5	82	0.25	2.7	D

Table 5.1 *Atmospheric conditions for trial case 4*

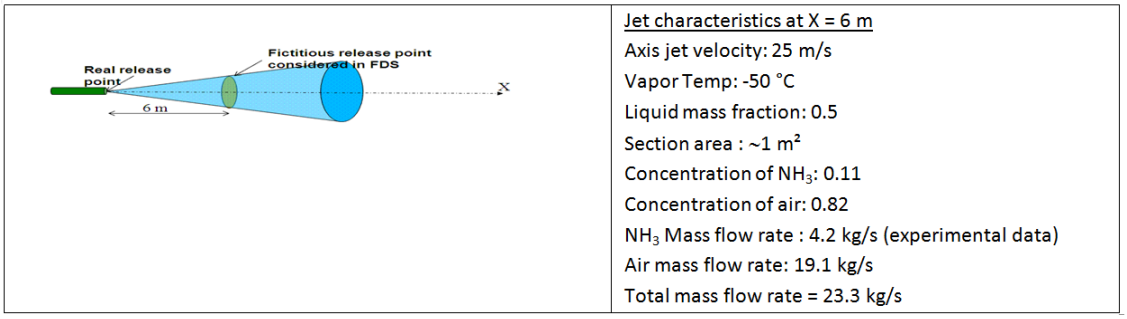

Figure 5.2 *Description of the source term implemented in FDS simulation*

near the testing site. It allowed recording the ambient temperature, the relative humidity and the solar flux at a height of 1.5 m. For all apparatus, the scanning frequency was set to 1 Hz except the ultrasonic anemometer whose frequency was adjusted to 10 Hz. Catalytic sensors (near field) and electrochemical cells (far field) allow to measure ammonia concentration. Sensors were positioned in 7 arc shapes centered on the release point (see Figure 5.1).

Several tests release cases were conducted with mass flow rate up to 4 kg/s. For the scope of the present study the trial case 4 is considered. It corresponds to a free field jet release. As expected, the ammonia cloud behaved like a heavy gas and no elevation of the cloud was observed. For a relative humidity of 82%, the visible cloud length was about 500 m. This visibility is associated with the condensation of water contained in the ambient air once the latter is entrained into the two-phase release. During these tests, it was found that the temperature of such release can drop down to -70°C. Once the cloud is sufficiently heated by dilution with ambient air, the cloud is no longer visible. The meteorological conditions is summed up in table 5.1.

5.2.2 Implementation of a biphasic and dense gas source term

FDS software cannot directly deal with multi-phase releases. In order to bypass this limitation, a simple methodology has been developed to achieve an equivalent term source. Papadourakis *et al.* [24] approach was previously used for computing source term, which is implemented as an equivalent source term in FDS simulation. A brief summary of this source term is given in Figure 5.2.

5.2.3 Adaptation of an experimental signal for input to LES

Previous CFD flow simulations with RANS approach show that better results are obtained when the inlet conditions are fitted to measurements both for mean velocity profile or for inflow turbulence

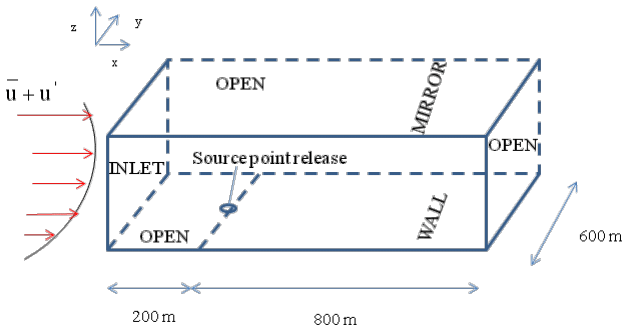

Figure 5.3 *The computational domain and the boundary conditions for the simulations.*

[25, 26]. Preliminary tests with FDS with mean velocity profile at inlet of the flow show that turbulence is not sufficiently generated inside the computational domain. This result is consistent with the physics of the LES model that consider instantaneous velocities for each component U, V and W. Within the context of this current experimental validation approach we intend to reproduce the experimental signal. In LES, the inlet condition is a definition of mean velocity and its temporal fluctuations. A power law is used to fit the mean wind module along the experimental vertical profile (1.5, 4 and 7 m). The wind velocity signal in time for FDS inlet boundary condition is obtained by performing a Fourier analysis in time on the experimental signal (reference point : 7 m on the mast). It allowed building the fluctuating wind velocity signal for the U and V components. The construction was performed by using an orthogonal transformation. The signal is then built on the basis of linear sum of cosine and sine functions (equation 5.1) with coefficients representing the energy contained in each mode (k).

$$u' = \sum_{k=1}^{n} a_k \cos(2\pi f_k t) + b_k \sin(2\pi f_k t) \tag{5.1}$$

In the numerical simulation, the 50 most significant coefficients were introduced in the inlet profile to reproduce U and V signal components in time. The coefficients are directly proportional to the turbulence intensity such that we ensure to introduce most of the turbulence information. Due to the lack of data along vertical axis, the fluctuating component of the velocity profile is taken proportional to the one at 7m and weighted by the mean velocity along the main wind direction. Therefore the turbulence intensity is constant along the vertical profile. This constitutes a strong hypothesis to characterize the inlet flow turbulence, however it seems less significant in the specific case of massive release located close to the ground. In summary, the 2D inlet boundary is set up by a homogeneous wind in space with no vertical component (W= 0 for all z). In this condition divergence free flow is satisfied. This approach corresponds to the simplest effective approach [27] to synthesize the inlet conditions for large eddy simulation. This approach is similar of Kondo *et al.* [28] approach, and developed by Shirani *et al.* [29]. Figure 5.3 presents the computational domain used in the calculations performed in the present study. Dimensions, source release location and boundary conditions are the main features shown. The calculation domain is defined by a single right parallelepiped mesh. This computational domain is 1000 m long with a grid cell size of 0.5 m in the near field of the release and of 1 m in the far field. Lateral and outlet boundaries are open boundaries. The ground is no-slip walls. The upper boundary is a mirror condition, i.e a free-slip wall.

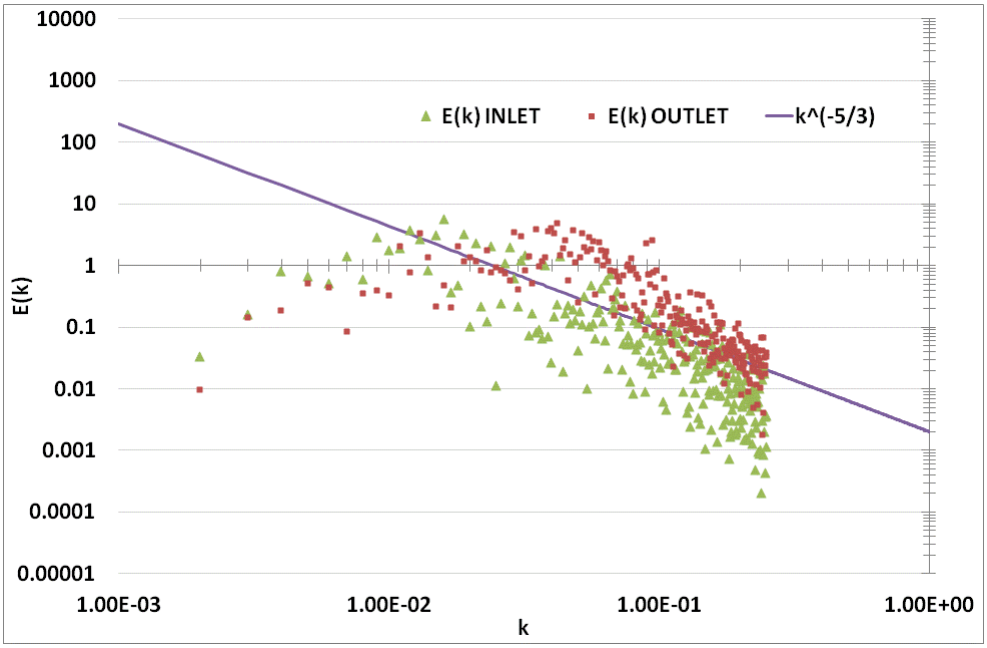

Figure 5.4 *Comparison of the turbulent energy spectrum from LES at the inlet and outlet conditions*

Simulations of the flow were performed before dispersion modeling of the release. A physical time of 1000 s is sufficient for FDS to generate a stabilized turbulence along the whole domain. The unsteady simulations were performed with a time step size automatically estimated according to the CFL requirement.

The Smagorinsky model was used for the LES computation. The value of the Smagorinsky constant C_s was 0.2. The time discretization is based on an explicit predictor-corrector scheme, that is first order accurate in space and time ensuring numerical stability. The second order scheme would be more accurate and is being tested. Simulations of the atmospheric flow without release were performed in order to observe the evolution of the spectra between the inlet and the outlet boundary. It shows a good conservation of spectra energy for the large scale spectral energy (Figure 5.4). However, a part of the energy has moved from the large to the small structures. This result is consistent with LES approach that aims to solve mainly the energy-containing motions.

5.2.4 Summary of the atmospheric dispersion results

The results of the ammonia release with the modeled atmospheric flow described in the previous section are briefly presented below. A rough comparison between modeling results and experimental observations shows that whole shape of the modeled cloud is in good accordance with experimental observations (see Figure 5.5). The modeled cloud of ammonia behaves as a dense gas for several hundred meters.

Figures 5.6 and 5.7 shows comparison between simulation results and experimental data for the whole set of receptors. Comparisons are performed with mean concentration. The averaging time roughly corresponds to the exposition time period defined by arrival time and departure time of the

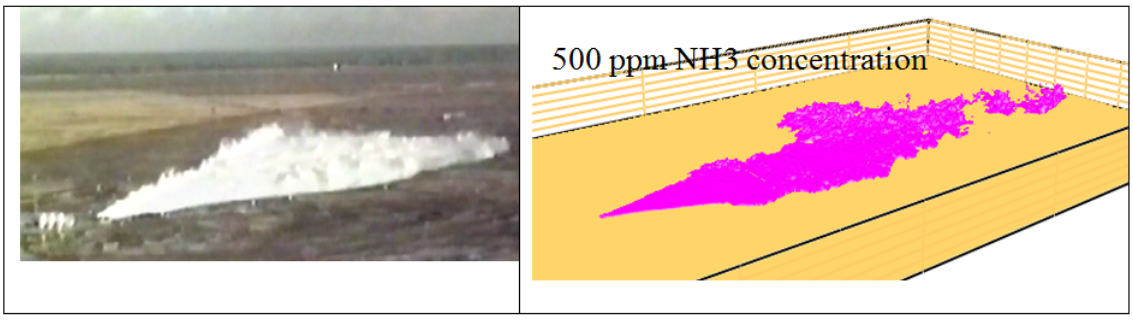

Figure 5.5 *Comparison between the overall form of the experimental cloud shape and simulation results*

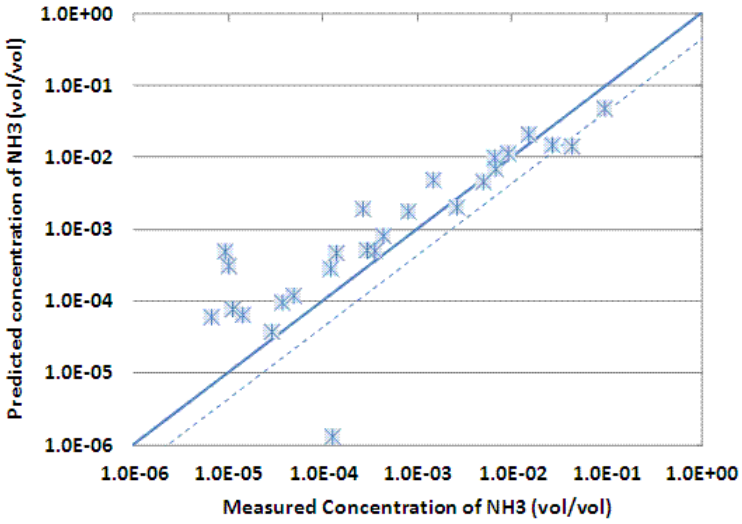

Figure 5.6 *Comparison between simulation results and experimental data for the whole set of sensors (logarithm scale)*

cloud. Taking into account the uncertainty of the sensor measurements, it is concluded that the modelling results are in good accordance with sensor measurements.

These promising results by LES approach are interesting regarding the complexity to describe both the release in the near field and the far field. Furthermore, the FDS code allows modelling the strong cooling effect of the release (as is observed experimentally). The necessity to set up a representative energy spectrum for the LES modelling has been shown in this experimental comparison.

5.3 Towards predictive modeling for stable conditions

An overwhelming variety of methods (recycling method, synthetic method, forcing method) aiming to generate inflow boundary conditions for LES [30] have been reviewed in the literature. The

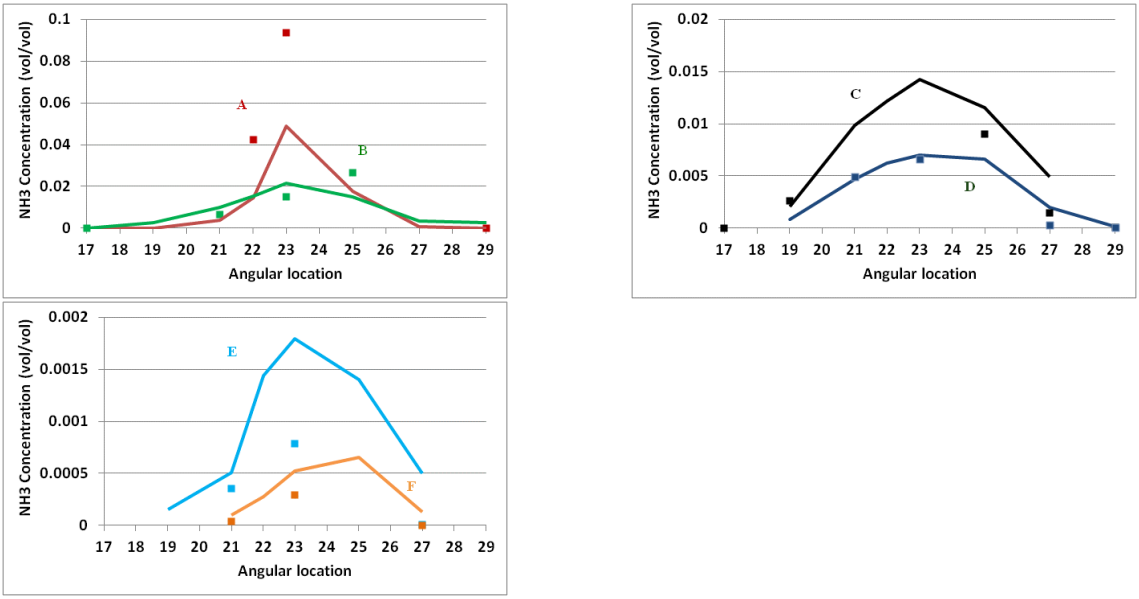

Figure 5.7 *Comparison between simulation results and experimental data for each arc (A, B, C, D, E, F) of sensors*

method of inlet generation for LES approach, presented in this chapter, appears as very simple. To go further it is worth using methods that introduce turbulence in space as well as in time. These methods are based on more statistical information of the flow turbulence. To reach this objective we propose to use experimental velocity data from SIRTA[3] [31] experiment that allow providing significant information on space and time correlation of the wind flow in case of atmospheric stable conditions. In order to harmonize the inlet flow between definitions usually assessed by Gaussian model or RANS modelling, the authors suggest to establish a link with turbulence characteristic used by more classical models or theoretical atmospheric classification such as the Pasquill stability classes.

[3]Site Instrumental de Recherche par Télédétection Atmosphérique.

6 Conclusions

The objective of this WP was to assess the possibility to provide a realistic source term for Liquefied Pressurized Gas (LPG) released from a vessel through a hole, or following a complete rupture, with CFD dispersion tools. This was investigated in four studies with different viewpoints.

It was stated that complete modelling of LPG release (liquid jet fragmentation, flashing of liquid aerosols, adiabatic expansion of the mixture of vapour and droplets, entrainment of surrounding air, droplet impacting on an obstacle, and rainout) is still out of reach of the capacities working in atmospheric CFD domain. Indeed, the dynamics involve time scales which differ by orders of magnitude. Compressibility effects, high turbulent production and dissipation at the jet exit, dispersed phase interacting with continuous gas mixture, and possible interaction with an obstacle complicates the picture further.

Obstacles close to the jet exit tend to cool rapidly when hit by a two-phase jet. The degree of cooling depends on the material, for instance obstacles of stainless steel cools down much more rapidly than obstacles of concrete (due to different heat capacities and thermal transfer coefficients). From the indoor experiment with the release of ammonia as a two-phase jet impinging a stainless steel plate positioned one meter from the release [9], a rainout fraction of 15% was measured. No rainout was observed for the corresponding pure NH_3 gas release. This effect has not been investigated in the modelling approaches presented here. It would require taking into account the heat transfer between the droplets and the gas and the wall, and to collect the liquid as a continuous phase (pool). One way to do this could be collecting the impacting droplets at a temperature below the boiling point, and generate a secondary source at the foot of the wall with the corresponding evaporation rate.

Another challenge for CFD modelling of the presented cases is that two-phase releases of ammonia will result in a dense gas source. This is due to the fact that evaporation of released liquid require heat from the entrained air, and this results in a cold air-vapour mixture which is denser than the ambient air. The dense gas acts to stratify the flow and thus suppresses the high turbulence levels of the jet locally. This is a challenge for CFD modelling.

In the first study (chapter 2), some conclusions (2.4) have been drawn regarding the use of RANS model for the flashing stage of the release process. The droplet distribution, mass fraction of vapour and liquid, inlet velocity and temperature were specified as inlet conditions for the simulation. Some difficulties emerged in the simulation: a very small time step was needed, making this method incompatible to further use in a large domain; furthermore a pressure-based solver was used, which helped to converge the flow field equation, but resulted in an overestimation of the energy and turbulence at the pipe exit. The evaporation of the liquid is believed to be captured, but the heat transfer by mixing with surrounding air was clearly underestimated.

The quasi-compressible LES model vida described in the second study (chapter 3) has been successfully utilized for the Jack Rabbit experiment for a genuine dense gas release with chlorine. The present study revealed that this model is not suited for the ammonia release. For the two-phase release, a two-way coupling between the gas solver and a lagrangian model for the liquid particles would be needed (to account for evaporation and the resulting dense gas effect), but currently only a one-way coupling from the gas phase to the liquid phase exists. For the gas release, the velocities

are to high for vida, as this is a low-mach solver. Instead a compressible LES solver, charles was tested. However, this solver is extremely time consuming and it was not feasible to simulate the full experiment. Furthermore charles does not allow several species, in other words it is not possible to simulate both ammonia vapour and air. Further development would be required to use these models for the ammonia scenarios.

The third study (chapter 4) presents a compromise between a full CFD simulation and a analytical approach, by decoupling the fast regime of the ammonia release from the subsequent slower dispersion regime. The former is handled by a source term model, while the latter by the "FOI Dispersion engine". Some encouraging validations have been made with FLADIS and INERIS experimental data. This would suit the requirement of a realistic source term for LPG release to be given as initial condition for subsequent CFD dense gas dispersion.

The last study (chapter 5) presents a LES approach where the inlet conditions for the release is specified by injecting a correlated and representative flow where the energy spectrum is based on the real profiles. The results are promising regarding the complexity for describing both the near field and the far field. In addition, the LES code allows to model the cooling effect by the evaporation of the released liquid. However, some more work is needed for validating the approach.

In conclusion, toxic industrial chemicals are often stored as pressurized liquid gases. A vessel failure or rupture gives a violent multiphase release of liquid and gas that the current CFD models used at DGA MNRBC (FR), INERIS (FR), FOI (SE) and FFI (NO) are not able to deal with in all its complexity. Interaction with an obstacle close to the release adds further to the complexity of the turbulent jet model; the impact on an obstacle and rainout of liquid to the ground is yet to be studied. However, it is currently possible to integrate part of the source empirically in CFD models by specifying the release rate, the liquid and gas mass fractions, the droplet distribution and the energy contents at the end of the expansion phase, and to compute the following dispersion and air entrainment. In order to handle a CFD source term such as a dense gas released from a ruptured vessel in an urban area, it is recommended to use an approach where the rapid phenomena (flashing and expansion) that need empirical descriptions, and slow phenomena (gas dispersion and entrainment) that can be CFD-computed, are decoupled.

Bibliography

[1] M Kiša and L' Jelemenský. Cfd dispersion modelling for emergency preparadnes. *Journal of Loss Prevention in Process Industries*, 22:97–104, 2009.

[2] H. W. M. Witlox and M Harper. Two-phase jet releases, droplet dispersion and rainout i. overview and model validation. *Journal of Loss Prevention in Process Industries*, 26:453–461, 2013.

[3] D M Deaves, s Gilham, B H Mitchell, P Woodburn, and A M Shepherd. Modelling of catastrophic flashing releases. *Journal of Hazardous Materials*, 88:1–32, 2001.

[4] R K Calay and Holdo A E. Modelling the dispersion of flashing jets using cfd. *Journal of Hazardous Materials*, 154:1198–1209, 2008.

[5] J L Woodward, Cook J, and A Papadourakis. Modeling and validation of a dispersing aerosol jet. *Journal of Hazardous Materials*, 44:185–207, 1995.

[6] P Bricard and L Friedel. Two-phase jet dispersion. *Journal of Hazardous Materials*, 59:287–310, 1998.

[7] A P van Ulden. On the spreading of heavy gas released near the ground, 1974. Proceedings Int. Loss Prevention Symp., pp 221226, C.H. Buschman ed., Elsevier, Amsterdam.

[8] Stephane Burkhart, Arnaud Gousseff, John Aa Tørnes, and Oscar Björnham. Moditic simulation report on operational urban dispersion modelling. FFR-rapport 2016/01299, The Norwegian Defence Research Establishment (FFI), 2016.

[9] O Gentilhomme. Moditic project: Agent characterisaton and source modelling. Report DRA-13-114532-08877A, INERIS, 2013.

[10] M Nielsen et al. Design of the fladis field experiments with dispersion of liquified ammonia. Technical report, Risø National Laboratory, 1994.

[11] M Nielsen and S Ott. Fladis field experiments final report. Technical report, Risø National Laboratory, 1996.

[12] S Duplantier. Analyse des conditions de dispersion d'un gaz liquéfié en champ proche en présence d'obstacles. Rapport INERIS SDu-2001, 2001. In French.

[13] TNO. Methods for the calculation of physical effects, CPR 14E, TNO Yellow Book. Ed. 2005.

[14] PA USA Fluent Inc., Canonsburg. Ansys fluent user's guide, 2016. from web.

[15] Thomas Vik, John Aa Tørnes, and Bjørn Anders P Reif. Simulations of the release and dispersion of chlorine and comparison with the jack rabbit field trials. FFR-rapport 2015/01474, The Norwegian Defence Research Establishment (FFI), 2015.

[16] A Shavit and C Gutfinger. *Thermodynamics: From Concepts to Applications*. CRC Press, second edition, 2008.

[17] S Fischer et al. Vådautsläpp av brandfarliga og giftiga gaser och vätskor: metoder för bedömning av risker. Technical Report FOA-R–97-00490-990, Swedish Defence Research Agency (FOA), 1997. In Swedish.

[18] G Polanco, A E Holdø, and G Munday. General review of flashing jet studies. *Journal of Hazardous Materials*, 173:2–18, 2010.

[19] F P Ricou and D P Spalding. Measurements of entrainment by axisymmetrical turbulent jets. *Journal of Fluid Mechanics*, 11:21–32, 1961.

[20] J O Hinze and B G van der Hegge Zijnen. Transfer of heat and matter in the turbulent mixing zone of an axially symmetrical jet. *Journal of Applied Scientific Research*, 1949.

[21] K B McGrattan. Fire Dynamics Simulator (version 4). Technical Reference Guide. NIST Special Publication 1018, NIST, 2005.

[22] Y Mouilleau and A Champassith. Cfd simulations of atmorpheric gas disperions using the Fire Dynamics Simulator (FDS). *Journal of Loss Prevention in the Process Industries*, 22:316–323, 2009.

[23] R Bouet. Rejets d'ammoniac: essais de dispersion atmosphérique à grande échelle. Technical Report DRA-Rbo-1999-20410, INERIS, 1999. In French.

[24] A Papadourakis, H S Caram, and C L Barner. Upper and lower bounds of droplet evaporation in two-phase jets. *Journal of Loss Prevention in the Process Industries*, 4:93–101, 1993.

[25] M Milliez and C Carissimo. Numerical simulations of pollutant dispersion in an idealized urban area, for different meteorological conditions. *Boundary-Layer Meteorology*, 122:321–342, 2007.

[26] M Milliez and C Carissimo. Copmputational fluid dynamical modelling of concentration fluctuations in an idealized urban area. *Boundary-Layer Meteorology*, 127:241–259, 2008.

[27] G R Tabor and M H Baba-Ahmadi. Inlet conditions for large eddy simulation: A review. *Computers & Fluids*, 39:553–567, 2010.

[28] K Kondo, S Murakami, and A Mochida. Generation of velocity fluctuations for inflow boundary condition of les. *Journal of Wind Engineering and Industrial Aerodynamics*, 67-68:51–64, 1997.

[29] E Shirani, J H Ferziger, and W C Reynolds. Mizing of a passive scalar in isotropic and sheared homogeneous turbulence. report TF-15, Mech. Eng. Dept., Stanford Univ., 1981.

[30] N Jarrin. Synthetic inflow boundary conditions for the numerical simulation of turbulence. Phd thesis, The University of Manchester, 2008.

[31] X Wei, E Dupont, B Carissimo, E Gilbert, and L Musson-Genon. A preliminary analysis of measurements from a near-field pollutants dispersion campaign in a stratified surface layer, 2013. Proceedings from the 15th International Conference on Harmonisation within Atmospheric Dispersion Modelling for Regulatory Purposes, Madrid, http://www.harmo.org/Conferences/Proceedings/_Madrid/publishedSections/H15-27.pdf.

About FFI

The Norwegian Defence Research Establishment (FFI) was founded 11th of April 1946. It is organised as an administrative agency subordinate to the Ministry of Defence.

FFI's MISSION

FFI is the prime institution responsible for defence related research in Norway. Its principal mission is to carry out research and development to meet the requirements of the Armed Forces. FFI has the role of chief adviser to the political and military leadership. In particular, the institute shall focus on aspects of the development in science and technology that can influence our security policy or defence planning.

FFI's VISION

FFI turns knowledge and ideas into an efficient defence.

FFI's CHARACTERISTICS

Creative, daring, broad-minded and responsible.

Om FFI

Forsvarets forskningsinstitutt ble etablert 11. april 1946. Instituttet er organisert som et forvaltningsorgan med særskilte fullmakter underlagt Forsvarsdepartementet.

FFIs FORMÅL

Forsvarets forskningsinstitutt er Forsvarets sentrale forskningsinstitusjon og har som formål å drive forskning og utvikling for Forsvarets behov. Videre er FFI rådgiver overfor Forsvarets strategiske ledelse. Spesielt skal instituttet følge opp trekk ved vitenskapelig og militærteknisk utvikling som kan påvirke forutsetningene for sikkerhetspolitikken eller forsvarsplanleggingen.

FFIs VISJON

FFI gjør kunnskap og ideer til et effektivt forsvar.

FFIs VERDIER

Skapende, drivende, vidsynt og ansvarlig.

FFI's organisation

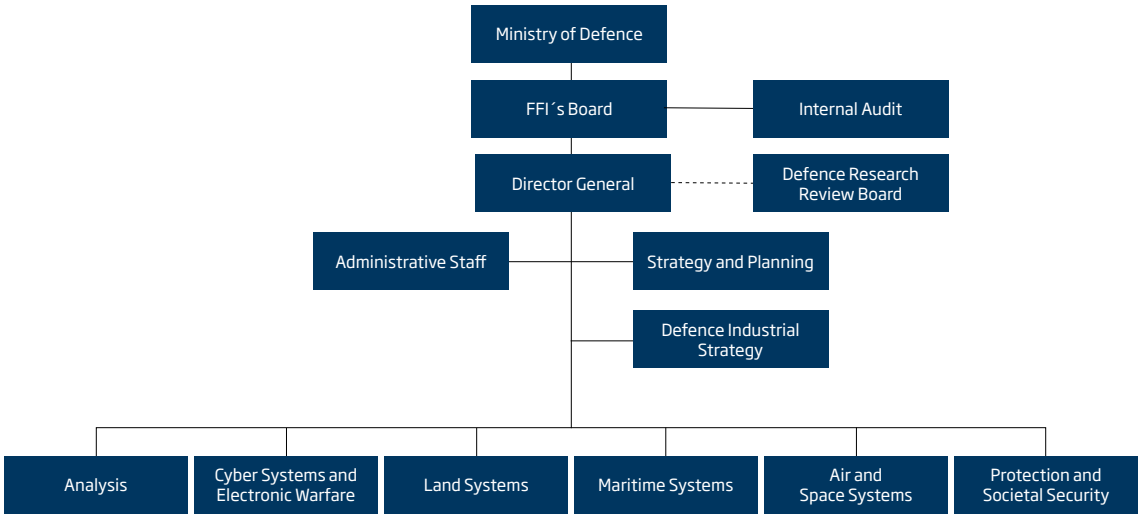

Forsvarets forskningsinstitutt
Postboks 25
2027 Kjeller

Besøksadresse:
Instituttveien 20
2007 Kjeller

Telefon: 63 80 70 00
Telefaks: 63 80 71 15
Epost: ffi@ffi.no

Norwegian Defence Research Establishment (FFI)
P.O. Box 25
NO-2027 Kjeller

Office address:
Instituttveien 20
N-2007 Kjeller

Telephone: +47 63 80 70 00
Telefax: +47 63 80 71 15
Email: ffi@ffi.no

FFI Forsvarets forskningsinstitutt
Norwegian Defence Research Establishment